

Kinematics of young stars (I): Local irregularities ^{*}

J. Torra, D. Fernández, and F. Figueras

Departament d'Astronomia i Meteorologia, Universitat de Barcelona, Av. Diagonal 647, E-08028 Barcelona, Spain

Received ;date; / Accepted ;date;

Abstract. The local velocity field of young stars is dominated by the galactic rotation, the kinematics of the Gould Belt and the nearest OB associations and open clusters, and the kinematics of the spiral structure. We re-examined here this local velocity field by using a large sample of nearby O and B stars from the Hipparcos Catalogue. The high quality astrometric data are complemented with a careful compilation of radial velocities and Strömgren photometry, which allows individual photometric distances and ages to be derived. The Gould Belt extends up to 600 pc from the Sun with an inclination with respect to the galactic plane of $i_G = 16\text{--}22^\circ$ and the ascending node placed at $\Omega_G = 275\text{--}295^\circ$. Approximately 60% of the stars younger than 60 Myr belong to this structure. The values found for the Oort constants when different samples selected by age or distance were used allowed us to interpret the systematic trends observed as signatures induced by the kinematic behaviour of the Gould Belt. The contribution of Sco-Cen and Ori OB1 complexes in the characterization of the expansion of the Gould Belt system is also discussed. We found that a positive K -term remains when these aggregates are excluded. From the kinematic behaviour of the stars and their spatial distribution we derive an age for the Gould Belt system in the interval 30-60 Myr.

Key words: Galaxy: kinematics and dynamics – Galaxy: solar neighbourhood – Galaxy: structure – Stars: early-type – Stars: kinematics

1. Introduction

The kinematic study of the local system of young stars offers an excellent opportunity for understanding the history of recent star formation and for improving our knowledge of the dynamics involved in the evolution of our galaxy.

Send offprint requests to: J. Torra

^{*} Based on data from the Hipparcos astrometry satellite (European Space Agency)

Correspondence to: jordi@am.ub.es

The motion of young nearby stars deviates considerably from the general field of galactic rotation (see e.g. du Mont 1977; Clube 1973). The presence of a positive K -term, corresponding to an overall expansion of the local system of the earliest stars was long ago (Campbell 1913) recognized as the main kinematic characteristic of the Gould Belt. This system is recognized to be a great circle inclined some 20° respect to the galactic equator and is traced by young stars and OB associations, HI, molecular clouds and dust. A detailed review of the structure, kinematics and origin of the Gould Belt has recently been undertaken by Pöppel (1997). Lesh (1968), Westin (1985) and Comerón et al. (1994; hereafter referred to as CTG) found, in addition to the positive K -value, departures from the values of other Oort constants when working with stars associated with the Gould Belt. In addition to the peculiar kinematics of the Gould Belt system, deviations from circular motion have also been analysed in the context of the kinematic effects of the spiral structure (Crézé & Mennessier 1973; Lindblad 1980; Byl & Ovensden 1981; Westin 1985; Comerón & Torra 1991, among others).

The publication of the Hipparcos data (ESA 1997) has made it possible to re-analyse the galactic velocity field and its local irregularities. Feast & Whitelock (1997) re-determined the mean values of the Oort constants from Hipparcos proper motion of Cepheids ($A = 14.8 \pm 0.8 \text{ km s}^{-1} \text{ kpc}^{-1}$, $B = -12.4 \pm 0.6 \text{ km s}^{-1} \text{ kpc}^{-1}$). Feast et al. (1998) obtained $A = 15.1 \pm 0.3 \text{ km s}^{-1} \text{ kpc}^{-1}$ by using radial velocities and the new zero-point period-luminosity relation from Hipparcos trigonometric parallaxes. Lindblad et al. (1997) and Torra et al. (1997) presented the first results concerning the structure and kinematics of the local system of young stars. Whereas Lindblad et al. (1997) do not rule out the possibility that the Gould Belt is just a random configuration of two or three dominating associations, Sterzik et al. (1998) and Guillout et al. (1998b), from a RASS-Tycho sample, suggest that the Belt is a disk-like rather than a ring-like structure. The Hipparcos census of nearby OB associations (de Zeeuw et al. 1999) and the review of the mean astrometric parameters of open clusters with Hipparcos (Robichon et al.

1999) have substantially increased our knowledge of the kinematic behaviour of the young stellar system in the solar neighbourhood.

In Sect. 2 we describe the samples we have used, based on the astrometric Hipparcos data plus a careful compilation of available radial velocities and Strömgren photometry. This information enables us to obtain reliable space velocities and individual ages for a large number of stars. In Sect. 3 a maximum likelihood method is applied in deriving the structural parameters and age of the Gould Belt. The velocity field was studied by means of the classical first-order approach in Sect. 4. The trends observed in the Oort constants are interpreted in terms of the expansion of the Gould Belt and the influence of stellar aggregates.

2. The working sample

Our initial sample (see Fernández 1998 for more details) contained 6922 O- and B-type stars (*Hipparcos Internal Proposal INCA060* completed with all the O and B *survey* stars), of which 5846 belong to the Hipparcos *survey*. The observational data were taken from the following sources:

- Astrometric data from the Hipparcos Catalogue (ESA 1997): positions in equatorial coordinates, parallaxes and proper motions, together with their standard errors and the correlations between them. Given the mean standard error in the trigonometric parallax provided by Hipparcos, reliable distances are available only up to 200-400 pc.
- Strömgren photometry from Hauck & Mermilliod's (1998) compilation for deriving individual photometric distances and ages.
- Radial velocities from Grenier's (1997) compilation plus additional sources.

In the following subsections we describe the procedure used and the accuracy achieved in the derivation of individual distances, spatial velocities and ages, together with a discussion of the possible observational biases present in the final working samples.

2.1. Stellar distances

To derive the best distance estimate for each star in the sample, an analysis of individual errors, possible observational biases and systematic differences between distances derived from Hipparcos trigonometric parallaxes and photometric absolute magnitudes was performed.

Only 3031 stars from our initial sample have complete Strömgren photometry ($b - y$, m_1 , c_1 , β and V) in Hauck & Mermilliod's (1998) catalogue. Recently, Kaltcheva & Knude (1998) found that photometric distances derived from Crawford's (1978) and Balona & Shobbrook's (1984) calibrations show good agreement with Hipparcos trigonometric distances, and that no dependence on star rotation

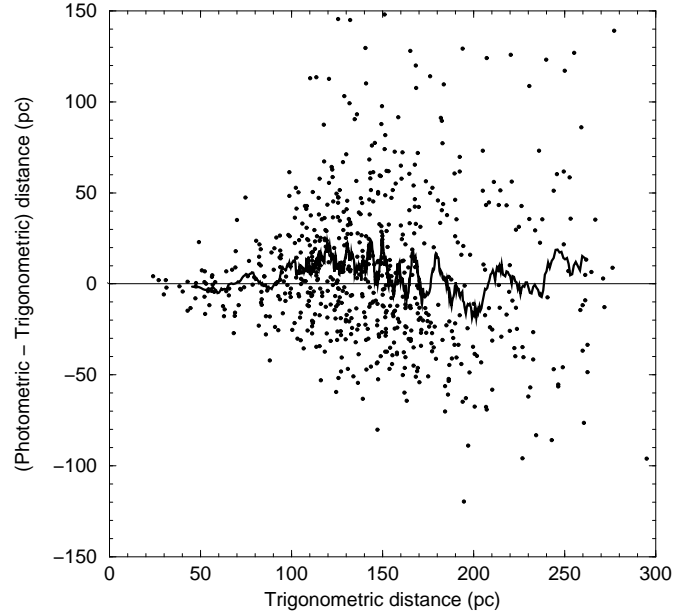


Fig. 1. Comparison of photometric and trigonometric distances for the sample stars with $\sigma_\pi/\pi < 0.15$. The solid line is a 25-point running average.

can be observed. The comparison of distances derived using Crawford's calibration and Hipparcos distances for the non-binary stars in our sample with $\sigma_\pi/\pi < 0.15$ (see Fig. 1) shows no systematic trends. We also verify that the use of another calibration (Balona & Shobbrook 1984; Jakobsen 1985) does not alter the kinematic results presented in Sect. 4. After this analysis, Crawford's (1978) calibration was adopted to derive photometric distances. A relative error in the photometric distance was computed following Lindroos (1981). Depending on the spectral type and luminosity class, this error ranges between 14-23%.

Reliable photometric distances can only be derived for single, non-variable and non-peculiar stars, so no photometric distance was derived for those stars classified as double or multiple in the Hipparcos Catalogue with a component separation $\rho < 10''$ and a magnitude difference between components $\Delta H_p < 3^m$, for variable stars with a variation in the Hipparcos magnitude system $\Delta H_p > 0.6^m$ and for stars photometrically classified as peculiar (Jordi et al. 1997).

For those stars for which we could obtain trigonometric and photometric distances, we used the distance with the smallest relative error. This procedure was preferred to the derivation of an error-weighted mean of both distance measurements since the latter would only systematically reduce the error for those stars around 150-250 pc (as will be seen in Sect. 4, this error is used as a weight in the condition equations, so a different weight would be assigned as a function of distance). Furthermore, negative trigonometric parallax or the bias in the trigonometric

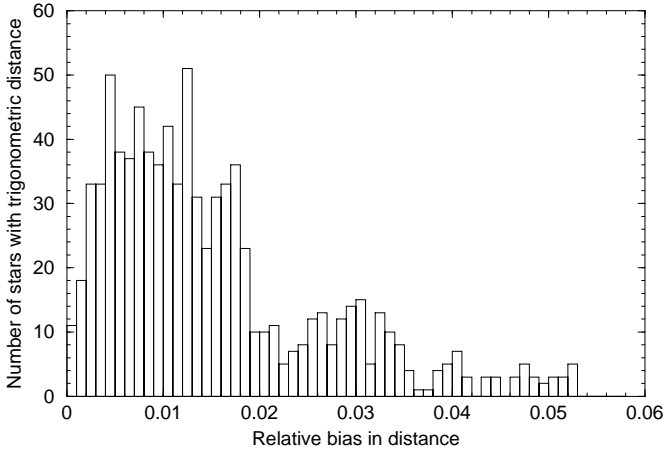


Fig. 2. Relative bias distribution for the 858 stars in our sample for which the trigonometric distance was chosen as providing the best distance determination.

distance discussed below – non negligible for stars with large relative error in parallax – could not be controlled.

In the case of stars for which the photometric distance was not available, to avoid bias, the trigonometric distance was only accepted if its relative error was smaller than 25%. If distances are estimated as $R = 1/\pi$, a symmetric error law for parallaxes results in a non-symmetric, biased distribution for distances. According to Arenou & Luri (1999), for small relative errors ($\lesssim 25\%$) and assuming a Gaussian law for the error on the observed parallax, this bias can be approximated by:

$$B(R) \approx \frac{1}{\pi_t} \left(\frac{\sigma_\pi}{\pi_t} \right)^2 \quad (1)$$

being π_t the *true* parallax. Individual corrections for the observed parallaxes are not possible because the bias is a function of the *true* parallax (Brown et al. 1997). However, an estimation of the effect of this bias in our trigonometric distances may be made considering in Eq. (1) the *observed* instead of the *true* parallaxes. In Fig. 2 we show the relative bias distribution ($B(R)/R$) for the 858 stars in our sample for which we chose the trigonometric distance as the best distance estimate. This relative bias is always less than 5.5%, and is smaller than 3% for 88% of the stars, thus giving a bias smaller than 5 pc for 82% of the stars. Therefore, given the impossibility of an individual correction of the biases, while recognizing their smallness (comparing, for instance, with the relative errors in the parallax), we may conclude that our assumption of considering directly the trigonometric distance as given by $R = 1/\pi$ for stars with relative error in parallax smaller than 25% is a good approximation.

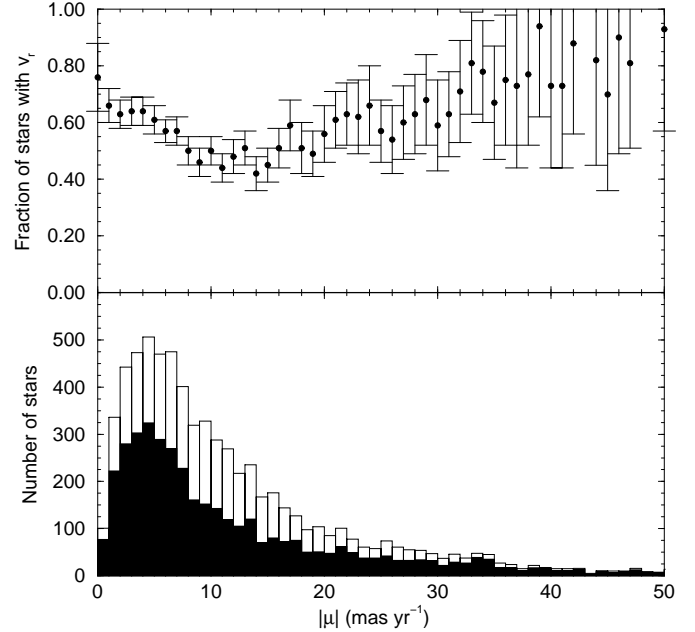


Fig. 3. Fraction of stars with radial velocity (top) and distribution of the stars with proper motion (blank histogram) and radial velocity (filled histogram) as a function of proper motion (bottom). Error bars were estimated from a Poissonian error distribution.

2.2. Stellar radial velocities

Our main source of radial velocities was the compilation of Grenier (1997), who made a complete compendium and revision of the compilations of Barbier-Brossat (1997) and Duflot et al. (1995). Priority was given to Barbier-Brossat, and only stars with A, B or C quality in Duflot et al. were considered. Using these sources, 3397 stars from our initial sample have radial velocity measurements. We rejected those stars with an individual error in the radial velocity higher than 10 km s^{-1} (131 stars, i.e. 3.9% of the stars with radial velocity).

Binney et al. (1998), when working with nearby stars from all spectral types, emphasized that, due to observational programmes, radial velocity availability is higher for high-proper motion stars. In our case, specific observational programmes were undertaken in parallel with the Hipparcos mission to obtain radial velocity data for *survey* early type Hipparcos stars. To evaluate the effects of the observational constraints on our kinematical study, we plotted in Fig. 3 the fraction of stars with known radial velocities (q_{vr}) against the total proper motion. We can see as this fraction is not a flat function of $|\mu|$: it decreases for $|\mu| \lesssim 10 \text{ mas yr}^{-1}$ and rises for $|\mu| \gtrsim 10 \text{ mas yr}^{-1}$. To understand this effect in Fig. 4 q_{vr} is shown against proper motion and distance. We can see a higher degree of completeness for distant stars. From Fig. 5 we derived a completeness limit of $V \approx 6.5$ for radial velocities, although nearly all far and faint stars ($R \gtrsim 1000 \text{ pc}$, so low

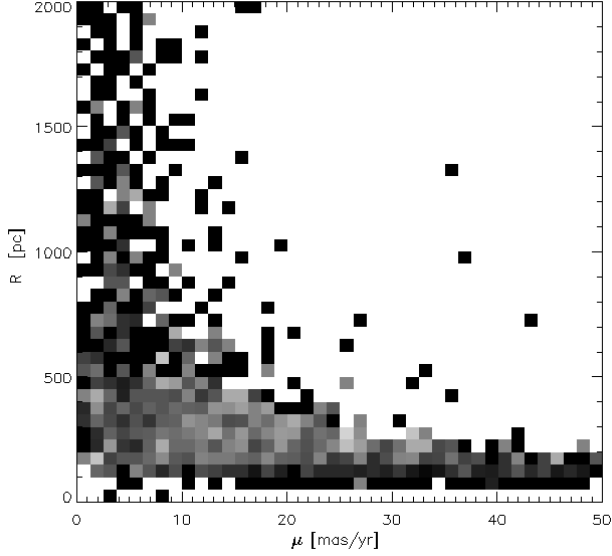


Fig. 4. Fraction of stars with radial velocity against proper motion and distance. This fraction is showed in a grey scale, from 0 (white) to 1 (black).

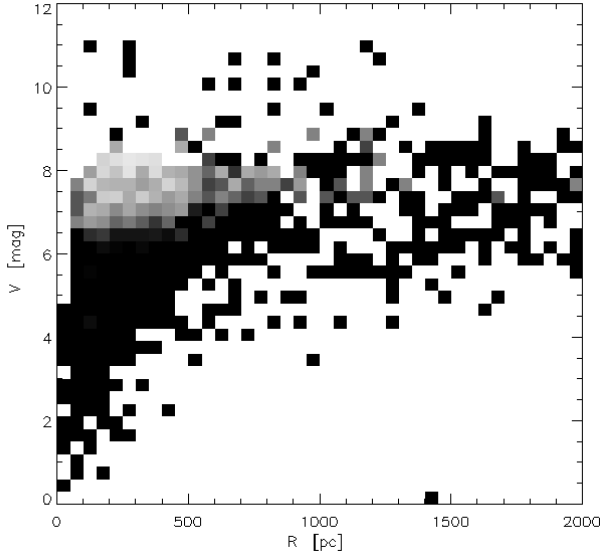


Fig. 5. Fraction of stars with radial velocity against distance and apparent visual magnitude. This fraction is showed in a grey scale, from 0 (white) to 1 (black).

$|\mu|$) have radial velocity data. A possible origin for this effect is due to observing programmes devoted to open clusters and associations. From this analysis we conclude that a kinematical bias is present in our sample and, although its effects on the analysis performed in Sect. 4 are expected to be negligible, they must be evaluated – see Appendix B: – through numerical simulations.

2.3. Stellar ages

Individual ages were computed from the evolutionary models of Bressan et al. (1993) for solar composition following the interpolation algorithm described in Asiain et al. (1997). The algorithm considers, as input parameters, the T_{eff} and $\log g$ derived from the Strömgren photometric indices (Moon et al. 1985; Napiwotzki et al. 1993).

The weakness in this procedure lies in the inability to take into account the effects of stellar rotation when deriving ages from photometry. Figueras & Blasi (1998), analysing a sample of main sequence B7-A4 stars, found that actual photometric ages increment by 30-50% in average, if rotation is not considered. As individual corrections are not possible, and an important fraction of the O-B9 main-sequence stars are high rotators, this important systematic trend has to be considered when deriving an age for the Gould Belt system.

First, individual ages were derived for all the stars for which photometric data was available, without taking into account binarity, variability or photometric peculiarities. The age and relative error in age distributions computed for 2864 stars are presented in Fig. 6 and Fig. 7, respectively. With the aim of retaining as many as possible of the very young stars in our final sample, a careful treatment was followed to take into account the effects of binarity, duplicity or peculiarity in the age computation:

- In the case of double or multiple stars for which only joint photometry is available (i.e., systems with $\rho < 10''$ and $\Delta H_p < 3^m$), the computed age is greater than the real age (Trimble & Ostriker 1981). All double or multiple systems with computed ages smaller than 30 Myr have an actual age inside the interval $\tau \leq 30$ Myr, so they were retained in the working sample only if they have a reliable Hipparcos trigonometric parallax ($\sigma_\pi/\pi < 0.25$), as the effects of duplicity render the photometric distance meaningless. Furthermore, roughly 80% of these stars have $\tau + \sigma_\tau \leq 60$ Myr, so there is a high probability that they belong to the Gould Belt. Double or multiple systems with an estimated age larger than 30 Myr were rejected.
- We rejected those stars with photometric or spectral peculiarities. The photometric indices accounting for temperature for Bp stars are bluer due to peculiarities, thus producing estimated ages smaller than real (Hauck 1975). Variable stars with $\Delta H_p > 0.6^m$ were also rejected.
- As shown in Fig. 7, about 12% of the sample has a relative error in age larger than 100%. From them, those placed below the ZAMS (206 stars) are peculiar stars that are already rejected or very young stars. We checked that the stars above the ZAMS had a computed age smaller than about 30 Myr (116 stars). In any case, as these stars are expected to be very young and therefore of great importance to our study of the Gould Belt (they represent roughly 25% of the stars

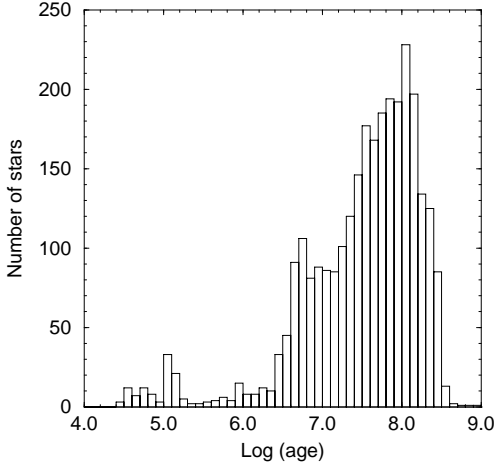


Fig. 6. Age distribution of the sample of O and B stars (2864 stars).

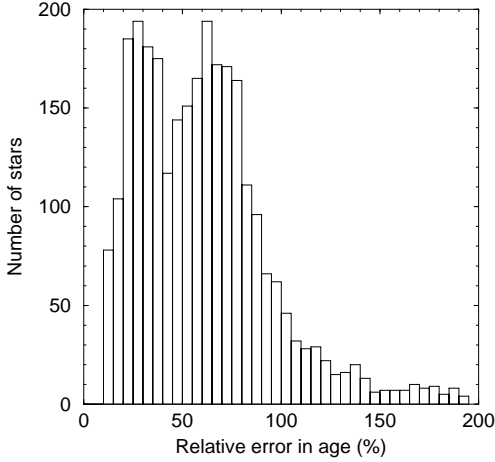


Fig. 7. Distribution of the relative error in age of the O and B stars in the sample. 88% of the stars have a relative error in age smaller than 100%.

Table 1. Averaged errors in the samples of O and B stars.

Error	Sample 1	Sample 2
$\overline{\sigma}_\pi$	0.60 mas	0.57 mas
$\left(\frac{\sigma_\pi}{\pi}\right)$	0.168	0.163
$\overline{\sigma}_{\mu_\alpha \cos \delta}$	0.83 mas yr ⁻¹	0.81 mas yr ⁻¹
$\overline{\sigma}_{\mu_\delta}$	0.70 mas yr ⁻¹	0.67 mas yr ⁻¹
$\overline{\sigma}_{v_r}$	—	3.44 km s ⁻¹

with $\tau \leq 30$ Myr), we decided to retain them in the final sample.

2.4. Working samples

Following the procedure described above, two samples of stars were formed:

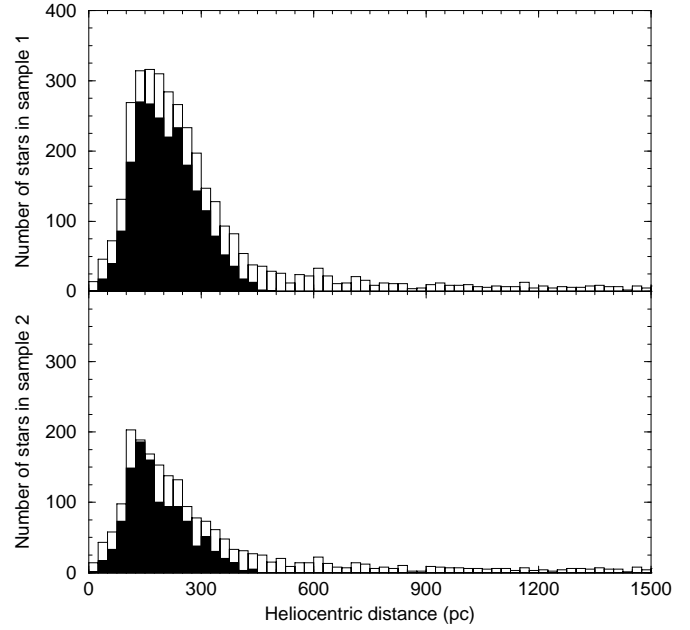


Fig. 8. Distance distribution of the samples 1 (top) and 2 (bottom) of O and B stars defined in the text. Filled histograms show the stars for which Hipparcos trigonometric distance was used (56.3% and 50.2% of the stars belonging to samples 1 and 2, respectively).

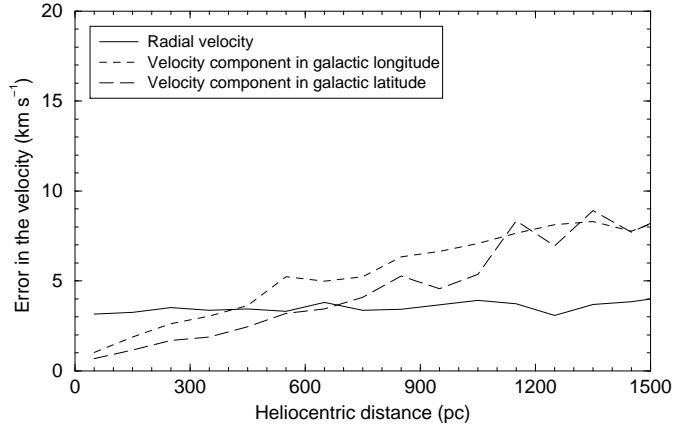


Fig. 9. Averaged errors in the three velocity components plotted against heliocentric distance.

- **Sample 1:** Containing 3915 stars with known distance and proper motions.
- **Sample 2:** A subsample of sample 1 containing 2272 stars with known distance, radial velocity and proper motions.

In Fig. 8 we show their distance distribution. Although the initial sample contains all the *survey* Hipparcos stars (complete up to $V = 7.9$), the lack of photometry and radial velocity data reduces the completeness of the samples to about $V_{\text{lim}} \approx 6.3$, that is up to 150 pc for a B9V star, the faintest in our sample.

The averaged errors of several quantities are presented in Table 1. In Fig. 9 we show the averaged errors in the three velocity components plotted against heliocentric distance (computed taking into account the correlations between the different variables provided by the Hipparcos Catalogue).

The number of stars in samples 1 and 2 is reduced to 2468 and 1789, respectively, when individual ages are required. In Fig. 10 we show the position of these stars projected on the X - Z plane (X positive towards the galactic center and Z towards the north galactic pole), classified in three age groups ($\tau \leq 30$ Myr, $30 < \tau \leq 60$ Myr and $\tau > 60$ Myr). The Gould Belt is recognized as a tilted structure with regard to the galactic plane ($Z = 0$), mainly in the region with $X < 0$ and $Z < 0$. This structure is clearly visible for stars younger than 60 Myr. The presence of some stars belonging to this structure in the interval $60 < \tau \leq 90$ Myr is fully justified by the large errors in the estimate of individual ages.

3. The Gould Belt

3.1. Structural parameters of the Gould Belt

A classic problem in the study of the Gould Belt has been how to separate the stars belonging to this structure from those belonging to the galactic belt. Stothers & Frogel (1974) and Taylor et al. (1987) proposed different algorithms based on the individual assignation of the stars to either belt. More recently, Cabrera-Caño et al. (1999; hereafter CEA) proposed *least mean classification error* decision criteria to separate those stars belonging to each belt. These criteria, based on the spatial distribution of the stars, run into an obstacle: the classification of stars lying in the overlap region between both belts.

In this paper, we followed an alternative approach proposed by CTG. The method assumes that the belts form two great circles in the celestial sphere, with a star density which decreases with the angular distance from each equator belt. The decrease in star density is assumed to follow a Gaussian law, the standard deviation being the angular halfwidth of the belt. Therefore, we suppose that the density distribution of the sample in the celestial sphere can be written as:

$$\sigma(l, b) = \sigma_G(l, b) + \sigma_g(l, b) \quad (2)$$

where σ_G and σ_g are the density distributions around the Gould Belt and the galactic belt equators, respectively.

This decomposition allows us to derive several parameters for the Gould Belt: the spatial orientation with regard to the galactic plane (i_G, Ω_G), the fraction of stars belonging to the Gould Belt (q), and the angular halfwidth of each belt (ξ_G, ξ_g). Comerón (1992), using pre-Hipparcos data, showed that the q parameter describes in an appropriate way the main characteristics of the distribution of young stars, in particular the extent of the belts as a function of galactic longitude.

The resolution procedure, based on the maximum likelihood method, can be found in Comerón (1992). Additionally, an iterative procedure until convergence was implemented here to minimize the dependence of the final results on the departing values. As explained in Comerón (1992), the method requires the homogenous completeness of the sample throughout over the entire celestial sphere. Unfortunately, although Hipparcos is complete up to $V = 7.9$, the absence of photometric measurements reduces this limit, so substantially reducing the distance limit of the intrinsically faint stars. As a good compromise between the constraints of completeness and the need for a statistically representative number of stars we considered only those stars that are brighter than $V = 7.0$ in sample 1. Numerical simulations, presented in Appendix A., allowed us both to assess how these incompleteness effects could influence the results and to have an external evaluation of the errors on the derived structural parameters.

The results obtained for the real sample are presented in Table 2. We see that the Gould Belt's structure is clearly detected in the subsamples of young stars with $R \leq 600$ pc. From the top left panel in Fig. 10 (stars with $\tau \leq 30$ Myr) we also see that this structure extends up to 600 pc into the south galactic hemisphere and only up to 200-300 pc in the north. As young stars in the galactic plane reach distances greater than 1000 pc without having any substantial decrease in density, we can state that the distance cut off derived for this structure is real in this age interval and not a consequence of the incompleteness of our sample. An extent of about 600 pc is in agreement with Lindblad et al. (1997), who assumed that the prominent associations in the Gould Belt are within a distance of 700 pc.

The orientation parameters were found to be $i_G = 16-22^\circ$ and $\Omega_G = 275-295^\circ$. The orientation parameters are maintained up to the interval 60-90 Myr. For stars older than 90 Myr the method does not converge – large errors are found for i_G and Ω_G , and q and halfwidths are undetermined –, so we conclude that the Gould Belt is no longer present. However, at this stage, it is mandatory to verify that the disappearance of the structure for older stars is not a consequence of our observational constraints (in our sample, stars with $\tau \approx 60$ Myr have a limited distance about 400 pc). Simulations show that distance cut off for these stars does not significantly disturb the determination of structural parameters. In other words, if a substantial number of stars with ages larger than 60 Myr would be present in the Gould Belt, our algorithm would be able to detect them from the number of stars available at present. The smaller i_G value derived in the interval 30-60 Myr compared with that obtained in the intervals $\tau \leq 30$ Myr and $60 < \tau \leq 90$ Myr has no explanation at present (it cannot be attributed to the sample distance horizon). From the simulations, an uncertainty of $3-6^\circ$ is expected for i_G in these age intervals. In any case, our values for the orientation parameters are in good agree-

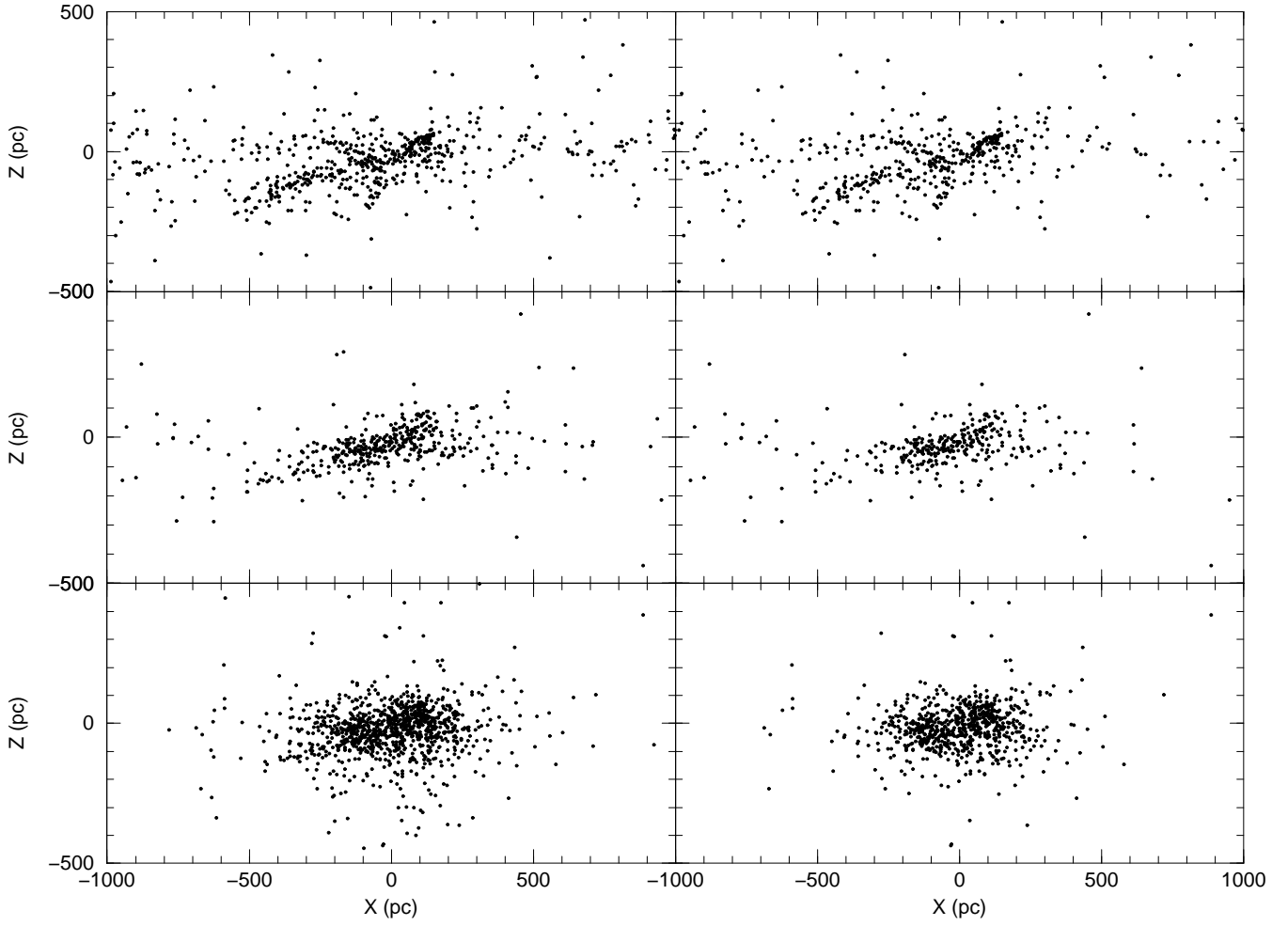


Fig. 10. Distribution on the X - Z galactic plane for the stars in the samples 1 (left) and 2 (right). At the top, the stars with an age less than 30 Myr; in the middle, those with an age between 30 Myr and 60 Myr; and at the bottom, those with an age larger than 60 Myr.

Table 2. Structural parameters of the Gould Belt as a function of distance and age: inclination (i_G), longitude of the ascending node (Ω_G), fraction of stars belonging to the Gould Belt (q), angular halfwidth of the Gould Belt (ξ_G) and the galactic belt (ξ_g), and number of stars (N). Limiting visual apparent magnitude: 7.0.

R (pc)	i_G ($^\circ$)	Ω_G ($^\circ$)	q	ξ_G ($^\circ$)	ξ_g ($^\circ$)	N
$\tau \leq 30$ Myr						
$R \leq 400$	21.2 _(1.3)	287.3 _(4.2)	0.60	6.2	22.5	236
$R \leq 600$	19.9 _(1.6)	282.8 _(5.2)	0.66	7.0	22.6	300
$600 < R \leq 2000$	11.8 _(2.2)	316.1 _(10.7)				126
$30 < \tau \leq 60$ Myr						
$R \leq 400$	15.9 _(2.5)	294.9 _(6.5)	0.64	7.3	23.7	261
$R \leq 600$	15.5 _(2.6)	293.4 _(6.5)	0.62	7.2	22.5	297
$600 < R \leq 2000$	11.9 _(22.7)	192.6 _(164.1)				31
$60 < \tau \leq 90$ Myr						
$R \leq 400$	22.3 _(2.1)	276.1 _(4.9)	0.44	7.6	25.8	177
$R \leq 600$	22.1 _(4.1)	276.7 _(4.1)	0.42	7.1	25.7	198
$90 < \tau \leq 120$ Myr						
$R \leq 400$	5.0 _(32.8)	316.7 _(378.4)				160
$R \leq 600$	3.4 _(33.8)	319.3 _(569.2)				170

ment with those published in the literature. Lesh (1968), Stothers & Frogel (1974) and Westin (1985) reported values of $i_G = 19\text{--}22^\circ$ and $\Omega_G = 270\text{--}300^\circ$. CTG reported $i_G = 22.3^\circ$ and $\Omega_G = 284.5^\circ$ from a sample of O-A0 stars. Recently, Guillout et al. (1998a) analysed the sky distribution of X-ray emitting stars belonging to the RASS-Tycho sample and found a low galactic latitude feature – the Gould Belt – with an orientation with regard to the galactic plane of $i_G = 27.5 \pm 1^\circ$ and $\Omega_G = 282 \pm 3^\circ$. Even if we take the errors into account, this inclination value is not compatible with ours. A possible explanation for this discrepancy is the fact that Guillout et al.'s sample was restricted to stars that were not located at such great distances ($R < 200$ pc), where the most prominent structure belonging to the Gould Belt – the Sco-Cen complex – defines a slightly higher slope than those located at a greater distance and in the opposite direction (mainly the Ori OB1 association). CEA, after identifying those stars belonging to the Gould Belt, found $i_G = 17.5\text{--}18.3^\circ$ and $\Omega_G = 287\text{--}294^\circ$, which is in very close agreement with our results.

For stars younger than 60 Myr, the fraction of stars belonging to the Gould Belt (q) were found to be 0.60–0.66. This value of q decreased to 0.42–0.44 when considering stars with an age between 60 and 90 Myr. From Appendix A: we expect an uncertainty of ≈ 0.15 in q . Therefore, its decrease for old stars must be real. CEA, classifying by spectral type groups, found $q = 0.44$ for O-B2.5 stars with $R < 1000$ pc, and $q = 0.36$ for O-B9.5 stars.

The angular halfwidths of the belts were found to be $\xi_G = 6\text{--}8^\circ$ and $\xi_g = 22\text{--}26^\circ$ (see Table 2) with an approximated uncertainty of 5° (see Appendix A:). These values tend to increase smoothly when we go from young to not so young stars. This effect, if real, could be simply due to the geometrical effect produced by the decrease in the mean distance when older stars are considered. We found that the Gould Belt is narrower than the galactic belt, contrary to the result obtained by CTG, and in perfect agreement with the relationship 1:3 obtained by Stothers & Frogel (1974) studying the scale heights for both belts. The same trend is observed in the paper by CEA.

3.2. The age of the Gould Belt

On the basis of the spatial distribution analysed in the previous section, and using individual photometric ages, we estimate the belt to be younger than 60 Myr. As explained before there are two major biases in the computation of individual photometric ages that account for the presence of certain stars belonging to the Gould Belt in the age interval 60–90 Myr. First, due to the significant uncertainties in the age computation, we expect that some stars with actual ages smaller than 60 Myr are included in this interval. Second, and more importantly, the fact that we cannot include the effects of stellar rotation on the age computation scheme means there is a systematic

increase that can be evaluated in 30–40 Myr (Figueras & Blasi 1998).

The age estimates for the Gould Belt found in the literature lie in the interval 20–90 Myr. Lesh (1968) found an age of 45 Myr when supposing two superposed stellar distributions, and 90 Myr when considering only one homogeneous population in expansion. Lindblad et al. (1973) suggested an age of 30–40 Myr, the system being born in a spiral arm. Franco et al. (1988) found an age of 60 Myr for the Orion and Monoceros molecular cloud complexes. Tsoumis & Fricke (1979) and Comerón & Torra (1991) reported 60 Myr and 70 Myr, respectively, from kinematic studies. From stellar individual age determinations using Strömgren photometry, Westin (1985) found an upper limit of 60 Myr. CTG divided their sample of O and B stars in spectral type subsamples, and reported a lower limit for age equal to the lifetime of a B4-type star (about 50 Myr). Guillout et al. (1998b), analysing the RASS-Tycho sample, reported the detection of a very young active late-type stellar population belonging to the Gould Belt. The X-ray luminosity distribution was compatible with an age of 30–80 Myr for these stars. More recently, Moreno et al. (1999) derived an age of 20 Myr, assuming that the Gould Belt was formed by an expanding shell.

A parallel determination of the Gould Belt's age from its kinematics will be given in Sect. 4.3.

4. Kinematics of young stars in the solar neighbourhood

4.1. Fit of the kinematic model

4.1.1. Equations for the linear model

The Oort constants were derived using the first-order development of the systematic velocity field:

$$\begin{aligned} V_r = & A R \sin 2l \cos^2 b \\ & + C R \cos 2l \cos^2 b + K R \cos^2 b \\ & - U_\odot \cos l \cos b - V_\odot \sin l \cos b - W_\odot \sin b \end{aligned} \quad (3)$$

$$\begin{aligned} R k \mu_l \cos b = & A R \cos 2l \cos b + B R \cos b \\ & - C R \sin 2l \cos b \\ & + U_\odot \sin l - V_\odot \cos l \end{aligned} \quad (4)$$

$$\begin{aligned} R k \mu_b = & -A R \sin 2l \sin b \cos b \\ & - C R \cos 2l \sin b \cos b - K R \sin b \cos b \\ & + U_\odot \cos l \sin b + V_\odot \sin l \sin b - W_\odot \cos b \end{aligned} \quad (5)$$

where l , b are the galactic coordinates, R the heliocentric distance in pc, V_r the radial velocity in km s^{-1} and μ_l , μ_b the proper motions in $'' \text{yr}^{-1}$ of each star. The constant k

$= 4.741 \text{ km yr (s pc } ^{-1})^{-1}$. U_{\odot} , V_{\odot} and W_{\odot} are the components of the peculiar motion of the Sun in km s^{-1} with regard to the circular velocity and A , B , C and K are the Oort constants, linear combinations of the gradients of the systematic velocity. No systematic motions perpendicular to the galactic plane were considered other than that arising from the solar peculiar motion. As recently verified by Palouš (1998), the E , D and H terms describing this systematic motion do not improve the results and their values are of low significance.

4.1.2. Resolution procedure

A weighted least squares fit was performed to estimate the model parameters from Eqs. (3), (4) and (5), taking the residual velocity of the star as a random error. Consequently, the weight of each equation was chosen as (Cr     1973):

$$p_i = \frac{1}{\sigma_{i,\text{obs}}^2 + \sigma_{i,\text{cos}}^2} \quad (6)$$

where σ_{obs} are the individual observational errors in each velocity component of the star, calculated by taking into account the correlations between the different variables provided by Hipparcos Catalogue, and σ_{cos} is the projection of the cosmic velocity dispersion ellipsoid (σ_{U} , σ_{V} , σ_{W}) in the direction of the velocity component considered. The detailed iterative procedure applied to simultaneously derive the model parameters and the cosmic dispersion for each of the subsamples considered is explained in Sect. 4.1.3.

To check the quality of the least-squares fits we considered the χ^2 statistics for $N - M$ degrees of freedom, defined as:

$$\chi^2 = \sum_{i=1}^N \frac{[y_i - y(x_i; a_1, \dots, a_M)]^2}{\sigma_{i,\text{obs}}^2 + \sigma_{i,\text{cos}}^2} \quad (7)$$

where x_i are the independent data (sky coordinates and distances), y_i the dependent data (radial and tangential velocity components), N the number of equations and M number of parameters to be fitted. According to Press et al. (1992), if the uncertainties (cosmic dispersion and observational errors) are well-estimated, the value of χ^2 for a moderately good fit would be $\chi^2 \approx N - M$, with an uncertainty of $\sqrt{2(N - M)}$.

To eliminate the possible outliers present in the sample due to both the existence of high residual velocity stars (Royer 1997) or stars with unknown large observational errors, we rejected those equations with a residual larger than 3 times the root mean square residual of the fit (computed as $\sqrt{[y_i - y(x_i; a_1, \dots, a_M)]^2 / N}$) and recomputed a new set of parameters. We checked that no more than 10-15 stars from the total sample were rejected using this procedure, so ensuring the objectivity of the rejection criterion.

Three distance intervals were considered: $100 < R \leq 600 \text{ pc}$, $600 < R \leq 2000 \text{ pc}$ and $100 < R \leq 2000 \text{ pc}$. The first two intervals allow us to determine the influence of the Gould Belt on the stellar kinematics, since as we have seen there is no evidence of the presence of this structure for $R > 600 \text{ pc}$. The last interval provides a global vision of the kinematics of young stars in the solar neighbourhood. Stars with $R \leq 100 \text{ pc}$ were not considered because, on the one hand, they do not give us information about galactic rotation and, on the other hand, peculiar motions of these nearby stars (small errors, so large weight) can disturb the results.

At this stage it is appropriate to clarify the physical meaning of the A , B , C and K terms in the two regions we want to analyse. In the region $600 < R \leq 2000 \text{ pc}$, not affected by the Gould Belt, these terms are expected to reflect the local shape of the rotation curve. Thus, assuming a smooth variation in space, they are properly called *Oort constants* and they account for the divergence (K), vorticity (B) and shear (A : azimuthally, C : radially) of the general velocity field of the galactic disk in the solar neighbourhood. Olling & Merrifield (1998) distinguished between *Oort constants* for the local shape of the rotation curve and *Oort functions* when accounting for their variation with the galactic radius. On the contrary, in the region $100 < R \leq 600 \text{ pc}$, these first derivatives of the velocity field will include the peculiar velocity field associated with the Gould Belt. Thus, strictly speaking, they should not be called *Oort constants* and so we will refer to them as *Oort parameters*.

Before analyzing the different fits performed there are two interrelated aspects that deserve special attention: the possible biases in the fitting parameters induced by the characteristics of the sample and our observational constraints – irregular spatial distribution of the stars, incompleteness effects, biases in the availability of radial velocity data (already discussed in Sect. 2.2), etc. – and the systematic errors in the parameters induced by the presence of observational errors in the right hand side of the Eqs. (3), (4) and (5), not considered in our least square fit. Cr     (1970) derived approximate analytical corrections to evaluate the second aspect but, as he stated, we think that numerical experiments are the best way to globally evaluate and discuss all the effects present in our real sample. Furthermore, these simulations can give us new insights in a long standing problem: the discrepancies appearing between the solutions obtained using radial velocity and proper motion equations. Following that, we performed several numerical simulations that are detailed in Appendix B. The results are commented, in the next paragraphs, along with the results from real data.

In Table 3, we compare the solutions obtained when considering only radial velocity data – Eq. (3) –, proper motion data – Eqs. (4) and (5) solved simultaneously – or the combined solution – Eqs. (3), (4) and (5) – for those stars in sample 2 with $600 < R \leq 2000 \text{ pc}$. As can be

Table 3. Oort constants and solar motion for stars in the sample 2 with $600 < R \leq 2000$ pc. Units: A, B, C, K in $\text{km s}^{-1} \text{ kpc}^{-1}$; $U_{\odot}, V_{\odot}, W_{\odot}, \sigma$ in km s^{-1} . χ^2/N_{eq} is the value of χ^2 divided by the number of equations. N is the number of stars. The errors in the fitted parameters were computed as $\sigma_i^2 = \sigma^2 C_{ii}^{-1}$, where $C_{ii}^{-1} = \text{Cov}_{ii}/\sigma^2$ is the corresponding element in the covariance matrix and σ the standard deviation of the measurements with unit weight (Linnik 1963). As expected, large errors in K and W_{\odot} are obtained when derived from proper motion data or radial velocity alone, respectively. A constant cosmic dispersion of $(\sigma_U, \sigma_V, \sigma_W) = (8, 8, 5) \text{ km s}^{-1}$ was considered in all cases.

Components	A	B	C	K	U_{\odot}	V_{\odot}	W_{\odot}	σ	χ^2/N_{eq}	N
$600 < R \leq 2000 \text{ pc}$										
V_r	11.7 _(1.1)		-0.7 _(1.1)	-3.0 _(0.7)	7.2 _(1.3)	16.6 _(1.2)	7.4 _(3.2)	14.3	2.64	308
$\mu_l + \mu_b$	14.5 _(0.9)	-12.8 _(0.6)	0.7 _(0.9)	-0.7 _(3.2)	10.7 _(1.0)	12.1 _(0.9)	8.5 _(0.5)	11.9	2.05	308
$V_r + \mu_l + \mu_b$	13.0 _(0.7)	-12.7 _(0.8)	0.0 _(0.7)	-3.3 _(0.7)	8.7 _(0.9)	14.1 _(0.8)	8.6 _(0.6)	12.7	2.39	308
$600 < R \leq 2000 \text{ pc}$ excluding the region with $200 < l < 250^\circ$										
V_r	14.0 _(1.6)		-1.0 _(1.2)	-1.4 _(1.0)	10.1 _(1.7)	18.5 _(1.6)	8.2 _(4.0)	15.1	2.91	224
$\mu_l + \mu_b$	13.5 _(1.1)	-11.8 _(0.9)	-1.1 _(1.4)	-9.4 _(4.2)	8.6 _(1.4)	13.7 _(1.3)	8.9 _(0.6)	13.1	1.19	224
$V_r + \mu_l + \mu_b$	13.5 _(1.0)	-11.4 _(1.0)	-1.1 _(0.9)	-2.3 _(0.9)	8.5 _(1.2)	15.8 _(1.0)	8.9 _(0.8)	13.5	1.25	224

seen, a difference about $2\text{--}3 \text{ km s}^{-1} \text{ kpc}^{-1}$ in the A value is present between the radial velocity and the proper motion solutions when solved separately. One effect that could reduce this discrepancy was pointed out by Cr  z   (1970): a non-negligible standard error in distances produces an underestimation of the A Oort constant when derived from radial velocities. Our numerical experiments (see Table B1) indicate that this effect is less important than the bias induced by the cut in the observed distance (affected by errors), which produces a bias of about $1\text{--}1.5 \text{ km s}^{-1} \text{ kpc}^{-1}$ in the opposite sense. From these simulations we conclude that the difference present in the real sample could even be enlarged if the observational bias could be removed.

Recently, Feast et al. (1998), working with a sample of Hipparcos Cepheids, showed that the discrepancy appearing between the A value derived from proper motions (Feast & Whitelock 1997) and that derived from radial velocities (Pont et al. 1994) disappears when the new Hipparcos Cepheid distance scale is considered in the last equations. In our case, we verified that an overestimation in our photometric distances by a factor of 20% – e.g. assuming a stellar rotation effect in the absolute magnitude derivation (Lamers et al. 1997, Domingo & Figueras 1999) – can account only for a difference of $1\text{--}2 \text{ km s}^{-1} \text{ kpc}^{-1}$ between both solutions.

Lindblad et al. (1997) attributed this discrepancy to the irregular distribution of stars and stellar groups and also to a possible non-linearity in the velocity field. As explained in Appendix B: our simulations take into account the irregular spatial distribution of real stars and we saw there that the discrepancy did not appear. More promising is the hypothesis that the discrepancies come from departures of some stellar groups from the adopted linear model. In our sample, we verified that when the stars in the region $200 < l \leq 250^\circ$ (partly composed by stars of the Ori OB1 and Col 121 associations) are removed, the dis-

crepancy on A vanishes (see Table 3). We also confirmed that when other special regions are removed, the discrepancy is maintained. Another important point we realize when studying these results is the variation in χ^2 statistics when rejecting those stars in this region. For proper motion data, χ^2/N_{eq} decreases from 2.1 to 1.2. On the contrary, for radial velocity data there is a little increase from 2.6 to 2.9. For the combined resolution a decrease from 2.4 to 1.3 was found. It seems indicate that there is a better fit of the velocity field to the model when rejecting this region. However, the value of χ^2/N_{eq} obtained is still larger than the derived in the simulations (see Appendix B:). This could be due by an underestimation in the error in the photometric distances and/or radial velocities for our stars.

Recently, Palou   (1998) used Hipparcos data to estimate the second-order terms in the expansion of the velocity field of young stars around the Sun. He concluded that these terms are always of low significance and do not significantly alter the values obtained for the first order derivatives (Oort constants). It cannot be ruled out that higher order terms might account for the irregularities observed, particularly the discrepancies appearing when some regions in l are omitted. However, the small number of stars available at large distances does not allow us to avoid the large correlations between variables when second order terms are included. We believe that the peculiar motions in certain specific regions are largely responsible for the discrepancies observed in the derivation of the A Oort constant.

Likewise, we confirmed that the discrepancy on V_{\odot} does not disappear when eliminating the stars of the Orion region, neither when eliminating stars from other regions. Again, from our simulations we discarded the irregular distribution of the stars in the $X\text{--}Y$ plane as an explanation for this discrepancy, so again the most probably explanation is the departure from the adopted model. Finally we

would to comment that the difference present in the derived K value is a simple consequence of the fact that this parameter is poorly determined when only proper motion equations of stars with small galactic latitude are considered.

Following we present the correlation matrices obtained for the radial velocities, proper motions and combined solutions given in Table 3:

i). Radial velocity solution:

A	C	K	U_{\odot}	V_{\odot}	W_{\odot}	
1.00	-0.12	-0.07	-0.18	-0.15	-0.12	A
	1.00	-0.03	0.05	-0.04	-0.00	C
		1.00	-0.11	-0.06	-0.09	K
			1.00	-0.08	-0.04	U_{\odot}
				1.00	-0.05	V_{\odot}
					1.00	W_{\odot}

ii). Proper motion solution:

A	B	C	K	U_{\odot}	V_{\odot}	W_{\odot}	
1.00	-0.14	0.11	-0.06	0.05	0.07	0.06	A
	1.00	0.14	0.03	-0.02	-0.15	-0.01	B
		1.00	0.04	-0.22	0.10	0.01	C
			1.00	-0.04	-0.08	0.24	K
				1.00	0.10	0.04	U_{\odot}
					1.00	0.05	V_{\odot}
						1.00	W_{\odot}

iii). Combined solution:

A	B	C	K	U_{\odot}	V_{\odot}	W_{\odot}	
1.00	-0.09	0.02	-0.07	0.07	0.08	0.01	A
	1.00	0.11	0.01	-0.02	-0.09	-0.01	B
		1.00	0.02	-0.10	0.02	-0.01	C
			1.00	-0.08	-0.07	0.01	K
				1.00	0.01	0.01	U_{\odot}
					1.00	0.05	V_{\odot}
						1.00	W_{\odot}

As can be seen, the correlations are small in all cases, constating that they are not responsible of the discrepancies between proper motions and radial velocities. We also realized that the combined solution presents the smallest correlations.

The information that can be derived from the χ^2 statistics provides us further arguments to favour the combined solution in the analysis performed in the following sections. As can be seen in Table 3, the worst values for the fraction χ^2/N_{eq} are obtained in the radial velocity solution, effect that is not reflected in our simulations. Two aspects can contribute to this fact: an underestimation of the observational errors in radial velocities – which can not be rule out since this parameter is very difficult to obtain for very hot stars – or an error in the adoption of the shape and size of the velocity dispersion ellipsoid. Both aspects will be discussed hereafter but the only way to fully analyze the cosmic dispersion velocity ellipsoid is through

Table 4. Standard deviation of the observational errors and cosmic dispersion for several subsamples divided in age intervals in the distance interval $100 < R \leq 600$ pc, both expressed in the galactic heliocentric coordinates system. $\sigma_{\text{cos}} = (\sigma_U^2 + \sigma_V^2 + \sigma_W^2)^{1/2}$: (1): this work, (2): Wielen (1977) analytical approximation $\sigma(t)^n = \sigma_o^n + C_v t$ with $n = 2$ and $C_v = 6 \cdot 10^{-7} (\text{km s}^{-1})^2 \text{yr}^{-1}$ and $\sigma_o = 10 \text{ km s}^{-1}$. Units: km s^{-1} .

Age (Myr)	$(\sigma_U, \sigma_V, \sigma_W)$	$(\sigma_U, \sigma_V, \sigma_W)_{\text{cos}}$	σ_{cos} (1)	σ_{cos} (2)
0 - 30	(3.5, 3.0, 2.3)	(7.9, 7.2, 4.3)	11.5	10.4
30 - 60	(3.1, 3.4, 1.8)	(6.2, 7.5, 4.4)	10.7	11.3
60 - 90	(3.2, 3.2, 2.0)	(7.5, 8.8, 4.5)	12.4	12.0
90 - 120	(3.2, 3.1, 2.1)	(10.9, 9.6, 6.4)	15.9	12.8
> 120	(3.2, 3.2, 2.9)	(10.8, 10.0, 5.5)	15.7	13.8

the residual analysis of the combined solution. Henceforth, we will work hereafter with the combined solution solving Eqs. (3), (4) and (5) simultaneously, so taking into account all the information available.

4.1.3. Cosmic dispersion

Our residuals in Eqs. (3), (4) and (5) include the observational errors, the residual velocity of the stars (cosmic dispersion) and possible departures from the adopted linear model. An optimal solution to characterize and separate the contribution of the cosmic dispersion may be to adopt it from independent works such as Wielen (1977), Lacey (1991), Asiain et al. (1999b), among others, who analytically or empirically evaluated the increase of the stellar velocity dispersion with age (disk heating). Discrepancies are present in the first 100-150 Myr (our working domain), where the population is not relaxed.

Working in the opposite sense, we can assume that the linear model adopted is approximately correct and that the observational errors are well estimated. With this hypothesis, and considering the interval $100 < R \leq 600$ pc to minimize both the possible departures from the lineal model and the observational errors, we solved the combined solution for different age intervals using an iterative process up to convergence. In all cases one iteration is sufficient and the results do not depend on the adopted initial values. The results are presented in Table 4.

We must point out that the values obtained for the Oort parameters and the solar motion components are practically independent of the choice of the cosmic dispersion values, the differences in these parameters being always smaller than $0.5 \text{ km s}^{-1} \text{kpc}^{-1}$ or 0.5 km s^{-1} respectively. Conversely, the adopted values for the cosmic dispersion will directly modify the χ^2 statistic. With this in mind, and the fact that the values derived for the cosmic dispersion are coherent with Wielen's work (see Table 4), we proceeded to solve combined solutions at different age intervals using the above explained iterative

process for the interval $100 < R \leq 600$ pc. For the interval $600 < R \leq 2000$ pc and $100 < R \leq 2000$ pc we use as cosmic dispersion the values obtained for $100 < R \leq 600$ pc, that is, assuming isothermality. This process give us the opportunity to use the χ^2 statistic to evaluate the over/underestimation of the observational errors or the departure from the adopted linear model. The results are summarized in Table 5 and discussed in the following sections.

4.2. Large scale outline of the local galactic kinematics

An initial overview of the kinematics of young stars in the solar vicinity is given when considering all the stars in the interval $100 < R \leq 2000$ pc. The solar motion relative to the stellar group considered was found to be:

$$(U_{\odot}, V_{\odot}, W_{\odot}) = (11.0, 12.9, 6.8) \pm (0.2, 0.2, 0.1) \text{ km s}^{-1} \quad (8)$$

On the other hand, we found the following values of the Oort constants, which are dominated by a pure differential galactic rotation:

$$\begin{aligned} A &= 11.8 \pm 0.4 \text{ km s}^{-1} \text{ kpc}^{-1} \\ B &= -12.3 \pm 0.4 \text{ km s}^{-1} \text{ kpc}^{-1} \\ C &= 0.4 \pm 0.4 \text{ km s}^{-1} \text{ kpc}^{-1} \\ K &= -2.0 \pm 0.4 \text{ km s}^{-1} \text{ kpc}^{-1} \end{aligned} \quad (9)$$

The kinematic distortion produced by the Gould Belt in the solar neighbourhood can be removed when considering only those stars with $600 < R \leq 2000$ pc. Then, we found a solar motion:

$$(U_{\odot}, V_{\odot}, W_{\odot}) = (9.0, 13.4, 8.3) \pm (0.8, 0.7, 0.5) \text{ km s}^{-1} \quad (10)$$

in perfect agreement with the classic value, the changes with respect to the former solution being partly produced by the presence of moving groups among young stars (Asiain et al. 1999a). From Appendix B: we expect these values to be slightly underestimated due to a bias of $\approx -(0.3-0.4) \text{ km s}^{-1}$. The Oort constants were found to be:

$$\begin{aligned} A &= 13.0 \pm 0.7 \text{ km s}^{-1} \text{ kpc}^{-1} \\ B &= -12.1 \pm 0.7 \text{ km s}^{-1} \text{ kpc}^{-1} \\ C &= 0.5 \pm 0.8 \text{ km s}^{-1} \text{ kpc}^{-1} \\ K &= -2.9 \pm 0.6 \text{ km s}^{-1} \text{ kpc}^{-1} \end{aligned} \quad (11)$$

From Appendix B:, a significant bias is only expected for B , with an underestimation (in absolute value) of about $0.8 \text{ km s}^{-1} \text{ kpc}^{-1}$. Therefore, its value might be $B \approx -12.9 \pm 0.7 \text{ km s}^{-1} \text{ kpc}^{-1}$. These A and B Oort constant values are in good agreement with the results obtained by Lindblad et al. (1997). Using Hipparcos data they found $A = 13.7 \pm 1.0 \text{ km s}^{-1} \text{ kpc}^{-1}$ and $B = -13.6 \pm 0.8 \text{ km s}^{-1} \text{ kpc}^{-1}$ from a sample of O and B stars with $R \leq 2000$ pc outside the Gould Belt. Feast & Whitelock (1997) reported $A = 14.8 \pm 0.8 \text{ km s}^{-1} \text{ kpc}^{-1}$ and $B = -12.4 \pm 0.6$

$\text{km s}^{-1} \text{ kpc}^{-1}$ from a sample of Cepheid stars (at distances up to 5000 pc) with Hipparcos proper motions and distance calibration. Using a similar sample (also with an Hipparcos distance calibration), Feast et al. (1998) found $A = 15.1 \pm 0.3 \text{ km s}^{-1} \text{ kpc}^{-1}$ from radial velocities. This tendency to obtain lower values for the A Oort constant when the distance horizon of the sample is approached is confirmed in the results presented in Table 5. Using stars with $100 < R \leq 600$ pc not belonging to the Gould Belt (age larger than 90 Myr), we found an A constant of $11.9 \pm 2.0 \text{ km s}^{-1} \text{ kpc}^{-1}$, roughly $1 \text{ km s}^{-1} \text{ kpc}^{-1}$ less than that obtained for all the stars with $600 < R \leq 2000$ pc. When comparing this result with the $A = 11.3 \pm 1.1 \text{ km s}^{-1} \text{ kpc}^{-1}$ derived by Hanson (1987) using proper motions for approximately 60 000 nearby faint stars ($R < 1000$ pc and a photographic magnitude $16 < m_{\text{pg}} < 17$) from the Lick Northern Proper Motion (NPM) program, we found a good coherence, although his sample was composed basically of F2-K0 stars. Recently, Olling & Merrifield (1998), using a mass model which includes the interstellar gas component, derived the variation in the Oort constants as a function of the galactocentric distance. The authors explained the discrepancies between the A values derived by Hanson (1987) and Feast et al. (1998) as being produced by the different mean galactocentric distances of the two samples. However, the authors admitted a potential source of error in their analysis due to the assumption of azimuthal symmetry in the orbital structure of the Galaxy.

Our nearly null values of C and K constants when considering all the stars in the distance intervals $100 < R \leq 2000$ pc and $600 < R \leq 2000$ pc are in good agreement with a pure differential galactic rotation. CTG found a value of $K \approx -(1-2) \text{ km s}^{-1} \text{ kpc}^{-1}$ for stars with $R < 1500$ pc, very similar to ours. Nevertheless, for the C constant they found a clearly negative value for B6-A0 stars: $C = -8.8 \pm 1.1 \text{ km s}^{-1} \text{ kpc}^{-1}$. This negative value of C seems to be corroborated by Mestres (1996), who found $C = -4.8 \pm 1.2 \text{ km s}^{-1} \text{ kpc}^{-1}$ for those stars with $400 < R \leq 1500$ pc. More recently, Lindblad et al. (1997) found $C = 0.8 \pm 1.1 \text{ km s}^{-1} \text{ kpc}^{-1}$ and $K = -1.1 \pm 0.8 \text{ km s}^{-1} \text{ kpc}^{-1}$ from their sample of O and B Hipparcos stars outside the Gould Belt. This last result is in very good agreement with ours.

To evaluate the goodness of our fit we can look at the χ^2 statistics. We found values 1.9-2.3 for χ^2/N_{eq} , depending on the age interval considered. For a moderately good fit we would expect a value $\chi^2/N_{\text{eq}} \approx 1$. We think the difference to be produced by an underestimation in the errors in the photometric distances and radial velocities for far stars.

This overall view is changed considerably when we divide our sample of stars into age and distance groups. The most characteristic change when we study the system of the nearest and youngest stars is the kinematic signature of the Gould Belt, i.e. the appearance of a non-null value

Table 5. Oort constants and residual solar motion as a function of distance and age. Units: Age in Myr; A , B , C , K in $\text{km s}^{-1} \text{ kpc}^{-1}$; U_{\odot} , V_{\odot} , W_{\odot} , σ in km s^{-1} . χ^2/N_{eq} is the value of χ^2 divided by the number of equations. N is the number of stars (sample 1 + sample 2).

Age	A	B	C	K	U_{\odot}	V_{\odot}	W_{\odot}	σ	χ^2/N_{eq}	N
100 < R ≤ 600 pc										
0 - 30	5.7 _(1.4)	-20.7 _(1.4)	5.2 _(1.4)	7.1 _(1.4)	8.1 _(0.5)	14.5 _(0.4)	6.4 _(0.3)	6.02	1.06	361 + 289
30 - 60	7.6 _(1.5)	-14.5 _(1.4)	9.5 _(1.6)	4.0 _(1.7)	11.6 _(0.4)	14.6 _(0.5)	7.4 _(0.3)	5.94	0.95	359 + 266
< 60	6.3 _(1.1)	-18.5 _(1.0)	5.9 _(1.1)	5.1 _(1.1)	9.8 _(0.3)	14.4 _(0.3)	6.9 _(0.2)	6.12	1.01	720 + 555
60 - 90	10.5 _(2.1)	-13.6 _(2.0)	5.9 _(2.1)	-5.4 _(2.3)	12.4 _(0.5)	13.8 _(0.6)	6.8 _(0.4)	6.72	1.14	245 + 183
> 60	11.8 _(1.5)	-11.0 _(1.4)	-0.9 _(1.5)	-3.5 _(1.7)	12.0 _(0.4)	13.2 _(0.4)	6.7 _(0.2)	8.07	1.09	932 + 654
> 90	11.9 _(2.0)	-9.4 _(1.8)	-4.6 _(2.0)	-1.9 _(2.2)	11.8 _(0.4)	12.9 _(0.4)	6.6 _(0.3)	8.30	1.09	687 + 471
All	8.8 _(0.8)	-14.2 _(0.7)	1.5 _(0.8)	0.5 _(0.9)	11.2 _(0.2)	13.0 _(0.2)	6.7 _(0.1)	7.24	1.06	2970 + 1596
600 < R ≤ 2000 pc										
0 - 30	13.3 _(0.7)	-11.7 _(0.7)	-0.3 _(0.7)	-2.6 _(0.7)	8.0 _(0.8)	12.9 _(0.8)	7.9 _(0.5)	10.39	1.95	285 + 204
30 - 60	9.1 _(1.7)	-10.8 _(1.8)	-3.4 _(1.8)	-0.8 _(1.8)	15.0 _(1.8)	10.4 _(1.7)	8.9 _(1.1)	11.57	2.29	81 + 56
< 60	12.7 _(0.6)	-11.7 _(0.7)	-0.6 _(0.7)	-2.5 _(0.6)	9.1 _(0.8)	12.5 _(0.7)	8.0 _(0.5)	10.91	2.05	366 + 260
All	13.0 _(0.7)	-12.1 _(0.7)	0.5 _(0.8)	-2.9 _(0.6)	9.0 _(0.8)	13.4 _(0.7)	8.3 _(0.5)	11.77	1.87	449 + 308
100 < R ≤ 2000 pc										
0 - 30	12.9 _(0.6)	-13.0 _(0.6)	0.5 _(0.6)	-1.7 _(0.5)	8.6 _(0.4)	13.4 _(0.4)	6.7 _(0.3)	7.85	1.51	646 + 493
30 - 60	9.6 _(1.0)	-13.2 _(1.0)	2.0 _(1.0)	-0.2 _(1.0)	11.7 _(0.4)	13.4 _(0.5)	7.4 _(0.3)	6.85	1.19	440 + 322
< 60	12.0 _(0.5)	-13.0 _(0.5)	0.7 _(0.5)	-1.5 _(0.5)	10.0 _(0.3)	13.4 _(0.3)	7.1 _(0.2)	7.52	1.34	1086 + 815
> 60	11.1 _(1.4)	-12.2 _(1.3)	-1.8 _(1.3)	-5.1 _(1.5)	11.8 _(0.4)	13.2 _(0.4)	6.8 _(0.2)	8.45	1.19	981 + 676
All	11.8 _(0.4)	-12.3 _(0.4)	0.4 _(0.4)	-2.0 _(0.4)	11.0 _(0.2)	12.9 _(0.2)	6.8 _(0.1)	7.77	1.17	3419 + 1904

of the K Oort constant and the peculiar behaviour of the other Oort constants.

4.3. Local irregularities: the kinematic effects of the Gould Belt

To study the kinematic characteristics of the Gould Belt, we present in Table 5 the results for those stars in our sample with $100 < R \leq 600$ pc. In Fig. 11, we show the variation of the Oort parameters with age. In general, we observe a marked increase in A and B values with age, and a decrease in C and K , according to the results obtained by Torra et al. (1997).

A non-pure differential galactic rotation was found for the youngest group of stars, with $A = 5.7 \pm 1.4 \text{ km s}^{-1} \text{ kpc}^{-1}$, $B = -20.7 \pm 1.4 \text{ km s}^{-1} \text{ kpc}^{-1}$ and non-null values for C and K . The tendency to obtain small A and B values for the youngest group is in perfect agreement with the results obtained by Lindblad et al. (1997) and Torra et al. (1997), although these authors even report negative A values in the combined solution. In agreement with these two studies, we confirmed that significant differences do appear in the solutions using only radial velocities or only proper motion equations ($A = 0.7 \pm 2.9 \text{ km s}^{-1} \text{ kpc}^{-1}$ and $A = 6.4 \pm 1.4 \text{ km s}^{-1} \text{ kpc}^{-1}$, respectively), and as discussed in the previous section, a possible explanation could be the departure of some stellar groups from the adopted linear model. When we considered not so young stars, A and B are closer to classic values ($A \approx 12 \text{ km s}^{-1} \text{ kpc}^{-1}$ and $B \approx -9 \text{ km s}^{-1} \text{ kpc}^{-1}$). From Appendix B: we can see that these differences are not expected to be

produced by any systematic bias. In this distance interval we only expect an underestimation in A of about $0.5 \text{ km s}^{-1} \text{ kpc}^{-1}$.

For those stars with $\tau \leq 60$ Myr we found a clear positive value of K -term: $K = 7.1 \pm 1.4 \text{ km s}^{-1} \text{ kpc}^{-1}$ for $\tau \leq 30$ Myr, and $K = 4.0 \pm 1.7 \text{ km s}^{-1} \text{ kpc}^{-1}$ for $30 < \tau \leq 60$ Myr. On the other hand, for stars older than 60 Myr slightly negative values of K were found – nearly compatible with a null value. Positive values of K were not found when we considered the distance interval $600 < R \leq 2000$ pc, independently of the age interval.

In the interval $100 < R \leq 600$ pc the obtained values for χ^2/N_{eq} were similar to those derived from the simulations (see Appendix B:), around 1.0. From the coherent values of the cosmic dispersion obtained, we can conclude that the velocity field of our stars fits the lineal model proposed and the errors are well estimated.

The variations in Oort parameters as a function of age allow us to infer an estimation of the age of the Gould Belt. As we have seen, when considering stars with $100 < R \leq 600$ pc a nearly pure differential galactic rotation was only found for stars with an age greater than 90 Myr. In the age interval 60-90 Myr, rather low values of A and B and a high value of C were still derived. So, we conclude that the age of the Gould Belt derived from the kinematic behaviour of the stars is in perfect agreement with that derived in Sect. 3.2 from the analysis of their spatial distribution.

In Fig. 12 we show the residual space velocity vectors for each star projected on the galactic plane, after subtracting the solar motion and the galactic rotation found

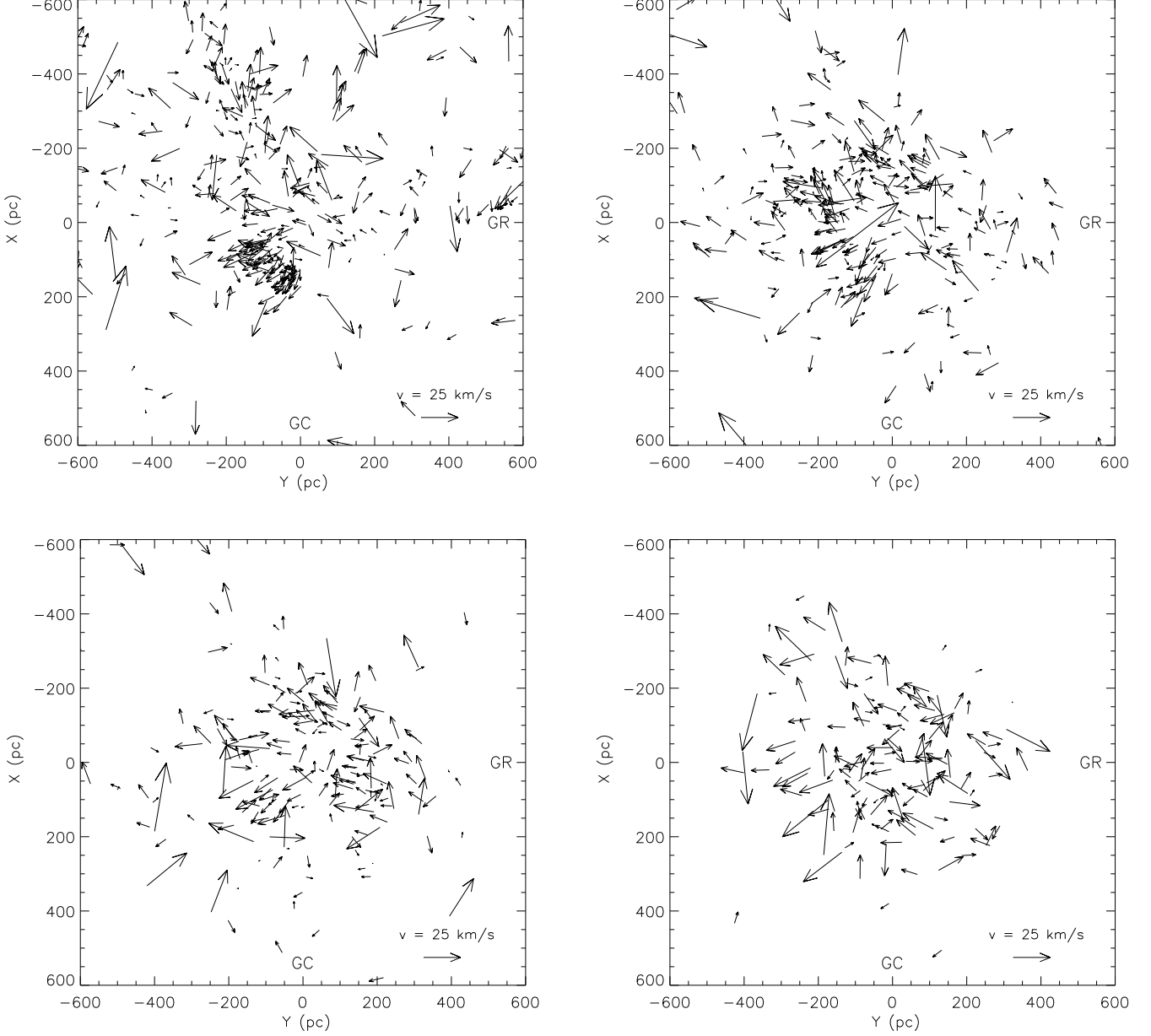


Fig. 12. Residual heliocentric space velocity vectors projected on the galactic plane for O and B stars with an age $\tau \leq 30$ Myr (top left), $30 < \tau \leq 60$ Myr (top right), $60 < \tau \leq 90$ Myr (bottom left) and $90 < \tau \leq 120$ Myr (bottom right).

Table 6. Oort parameters and residual solar motion for stars with $100 < R \leq 600$ pc and $\tau \leq 30$ Myr when excluding those stars belonging to the complexes Sco-Cen and Ori OB1, following the member lists provided by Brown et al. (1994; Ori OB1 association) and de Zeeuw et al. (1999; Sco-Cen complex). Units: A, B, C, K in $\text{km s}^{-1} \text{kpc}^{-1}$; $U_{\odot}, V_{\odot}, W_{\odot}, \sigma$ in km s^{-1} . χ^2/N_{eq} is the value of χ^2 divided by the number of equations. N is the number of stars (sample 1 + sample 2).

Excluded	A	B	C	K	U_{\odot}	V_{\odot}	W_{\odot}	σ	χ^2/N_{eq}	N
None	5.7 _(1.4)	-20.7 _(1.4)	5.2 _(1.4)	7.1 _(1.4)	8.1 _(0.5)	14.5 _(0.4)	6.4 _(0.3)	6.02	1.06	361 + 289
Sco-Cen	6.9 _(1.6)	-19.7 _(1.6)	4.7 _(1.6)	5.8 _(1.6)	8.5 _(0.6)	13.9 _(0.5)	6.2 _(0.3)	6.39	1.18	305 + 238
Ori OB1	6.1 _(1.6)	-20.7 _(1.6)	5.3 _(1.6)	7.3 _(1.6)	8.0 _(0.5)	14.6 _(0.4)	6.6 _(0.3)	6.14	1.10	315 + 251
Both complexes	7.2 _(1.8)	-19.7 _(1.8)	4.9 _(1.9)	6.0 _(1.9)	8.4 _(0.6)	14.0 _(0.6)	6.4 _(0.3)	6.60	1.26	258 + 200

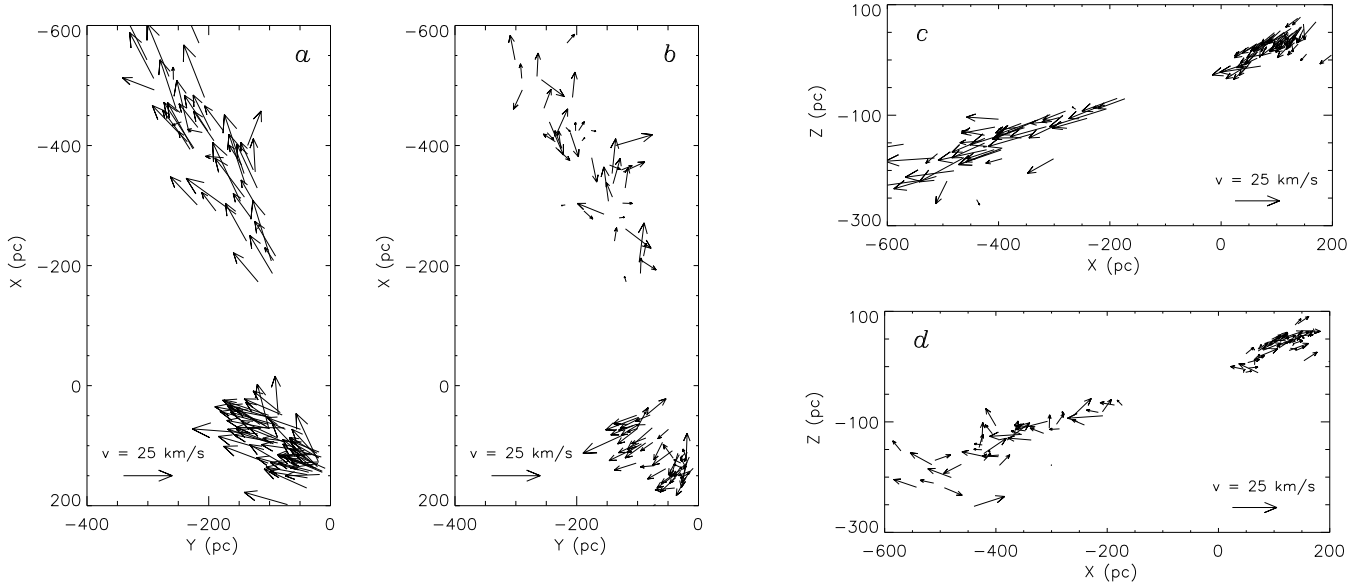


Fig. 13. Heliocentric space velocity vectors (*a,c*) and residual velocity vectors (*b,d*) projected on the galactic plane (*X-Y*) and the meridional plane (*X-Z*) for stars younger than 30 Myr belonging to the complexes Sco-Cen and Ori OB1.

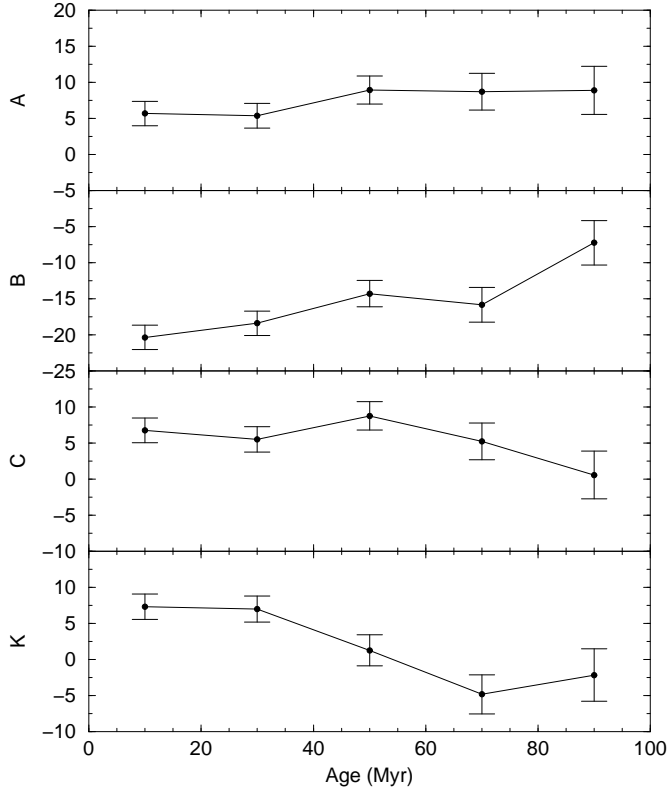


Fig. 11. Variation of Oort parameters plotted against the age for stars within $100 < R \leq 600$ pc. Units are in $\text{km s}^{-1} \text{kpc}^{-1}$.

in the resolution for all the stars in the distance interval $600 < R \leq 2000$ pc, classified in different age groups. From

this figure, it is evident that to model the expansion of the Gould Belt system as an expansion from a point (Olano 1982) or a line oriented in the direction $l = 45^\circ \rightarrow 225^\circ$ (CTG) is not a good approximation. In the same figure we have identified certain clumps associated with Lac OB1, Cep OB2, Cas-Tau, Per OB2, Col 121, Vel OB2, Tr 10 and Sco-Cen. All these associations, except Cep OB2, possibly belong to the Gould Belt (Comerón 1992; Pöppel 1997). In the youngest group (top left panel: stars with $\tau \leq 30$ Myr) we observe the clear residual motion of the Sco-Cen complex. This complex is composed of three associations – Upper Scorpius, US; Upper Centaurus Lupus, UCL; and Lower Centaurus Crux, LCC – at a distance of about 120-145 pc, in the region of positive *X* and negative *Y*. The Ori OB1 association shows a smaller mean residual motion, as will be discussed later. It is composed of several subgroups, situated in a range of distances of about 340-510 pc, in the direction of $l \approx 200\text{-}210^\circ$.

Sco-Cen and Ori OB1 are the two main complexes in the Gould Belt, and it is particularly interesting to study their motion and influence on the velocity field separately. This study might clarify whether the Gould Belt is a casual arrangement of OB associations or a structure with a common origin. In Fig. 13 we show the heliocentric velocity field and the residual velocity field – computed as in Fig. 12 – of the stars belonging to the Sco-Cen and Ori OB1 complexes on the *X-Y* and *X-Z* galactic planes. To select these stars, we used the member lists provided by Brown et al. (1994; Ori OB1 association) and de Zeeuw et al. (1999; Sco-Cen complex). It should be noted that we have detected – especially in the case of Sco-Cen – some additional stars whose location and kine-

matics are compatible with membership to these associations. We confirmed a high residual velocity field for Sco-Cen, which is moving away from the Sun: $(U, V, W)_{\text{res}} = (4.1, -6.7, 2.2) \text{ km s}^{-1}$, $(v_r, v_l, v_b)_{\text{res}}^1 = (7.1, -3.2, 0.6) \text{ km s}^{-1}$. In the case of the Ori OB1 association, the mean residual motion found was smaller and practically null in the radial direction: $(U, V, W)_{\text{res}} = (-2.7, 3.1, 3.6) \text{ km s}^{-1}$, $(v_r, v_l, v_b)_{\text{res}} = (0.2, -3.9, 3.8) \text{ km s}^{-1}$. These effects were confirmed when deriving the Oort parameters for those stars with $100 < R \leq 600 \text{ pc}$ and younger than 30 Myr not identified as members of these complexes (see Table 6). When Ori OB1 was excluded from the calculation of Oort parameters, the value of the K -term was found to rise only by $0.2 \text{ km s}^{-1} \text{ kpc}^{-1}$. In contrast, when Sco-Cen was excluded a decrease of $1.3 \text{ km s}^{-1} \text{ kpc}^{-1}$ in the K value was found. In both cases the A , B and C Oort parameters change less than about $1 \text{ km s}^{-1} \text{ kpc}^{-1}$. When both complexes were eliminated the parameters obtained were very similar to those obtained earlier (all the changes are within the error bars).

We conclude that these associations are not the only responsible for the peculiar kinematics observed for the youngest stars in the solar neighbourhood, attributed to the Gould Belt. So, other nearby associations and field stars belonging to the Gould Belt have a great significance in the determination of the Oort parameters.

An attempt was made at analysing the expansion of the system as a function of distance. As a first step, in Fig. 14 we present the variation of the KR product as a function of heliocentric distance for stars with $\tau \leq 60 \text{ Myr}$. The radial expansion diminishes rapidly with increasing distance (for $R < 250 \text{ pc}$) and it does not extend further than 400 pc. At distances larger than 300 pc, only Per OB2 has a mean residual motion away from the Sun. As discussed above, Ori OB1 has an almost null radial residual motion. Even considering the solar motion proposed by Dehnen & Binney (1998) – $(U_{\odot}, V_{\odot}, W_{\odot}) = (10.00, 5.25, 7.17) \text{ km s}^{-1}$ – and the galactic rotation curve obtained by Feast & Whitelock (1997), we obtain a small residual motion for this aggregate of $(U, V, W)_{\text{res}} = (-1.2, -2.8, 2.1) \text{ km s}^{-1}$, $(v_r, v_l, v_b)_{\text{res}} = (1.7, 1.9, 2.8) \text{ km s}^{-1}$. To analyse in more detail the expansion in the $R < 300 \text{ pc}$ region, we show in Fig. 15 the residual velocity vectors projected on the galactic plane for stars with $\tau \leq 60 \text{ Myr}$ (for clarity we divided the sample in two different coronae: $R \leq 150 \text{ pc}$ and $150 < R \leq 300 \text{ pc}$) together with Olano's (1982) Lindblad Ring – with a center placed at $R = 166 \text{ pc}$ from the Sun in the direction $l = 131^\circ$, and semiaxes of 364 pc and 211 pc – and the position of the center of the Gould Belt proposed by Comerón & Torra (1991) – $R = 80 \text{ pc}$, $l = 146^\circ$. In the first quadrant there is a lack of stars, partially produced by the near high extinction structures related to the Ophiuchus-Aquila complex (Vergely et al. 1997), which does not allow us to study the residual ve-

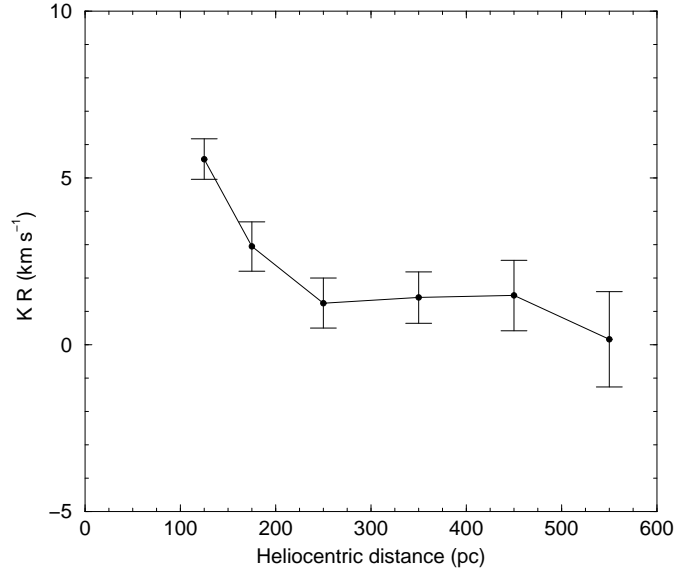


Fig. 14. Variation of KR against the heliocentric distance for stars with an age smaller than 60 Myr.

locity field in this region. The Cas-Tau complex is moving in the direction $l \approx 240^\circ$. So, as shown in Figs. 12 and 15 and by Lindblad et al. (1997), the third and fourth galactic quadrants contain the most significant structures accounting for the expansion of the Gould Belt.

Whereas the fourth quadrant contains the extensively studied Sco-Cen aggregate, a well-defined concentration of O and B stars with two different residual motions is present in the region $225 \lesssim l \lesssim 285^\circ$, mainly with distances in the interval $100 \lesssim R \lesssim 300 \text{ pc}$ and ages between 30 and 60 Myr. To analyse these streams in detail we present in Fig. 16 the distribution of these stars in the U - V plane, where a kernel estimator (Silverman 1986) was used to indicate the isocontours. Over this figure, the mean (U, V) heliocentric velocity components of the open clusters present in this region derived from Hipparcos data by Robichon et al. (1999) and the new kinematic structures recently identified by Platais et al. (1998) were also plotted. The stream placed at $(U, V) = (-12, -23) \text{ km s}^{-1}$ shares the motion of the a Car (= HIP 45080) cluster and IC 2602 open cluster, and it may also be related to the Pleiades moving group substructures found by Asiain et al. (1999a). The concentration observed at $(U, V) = (-28, -20) \text{ km s}^{-1}$ is associated with NGC 2451 A and Tr 10. The nature of NGC 2451 has been under discussion for some time. According to Röser & Bastian (1994), NGC 2451 can be divided into two different entities. These authors named the closest of these the Puppis Moving Group (PMG), the center of its distribution being clearly offset from the nucleus of NGC 2451 by 1° . The distance to PMG was found to be 220 pc. Carrier et al. (1999) also found two entities, at 198 and 358 pc respectively, from Geneva photometry and Hipparcos data.

¹ $v_l = 4.741 R \mu_l \cos b$ and $v_b = 4.741 R \mu_b$

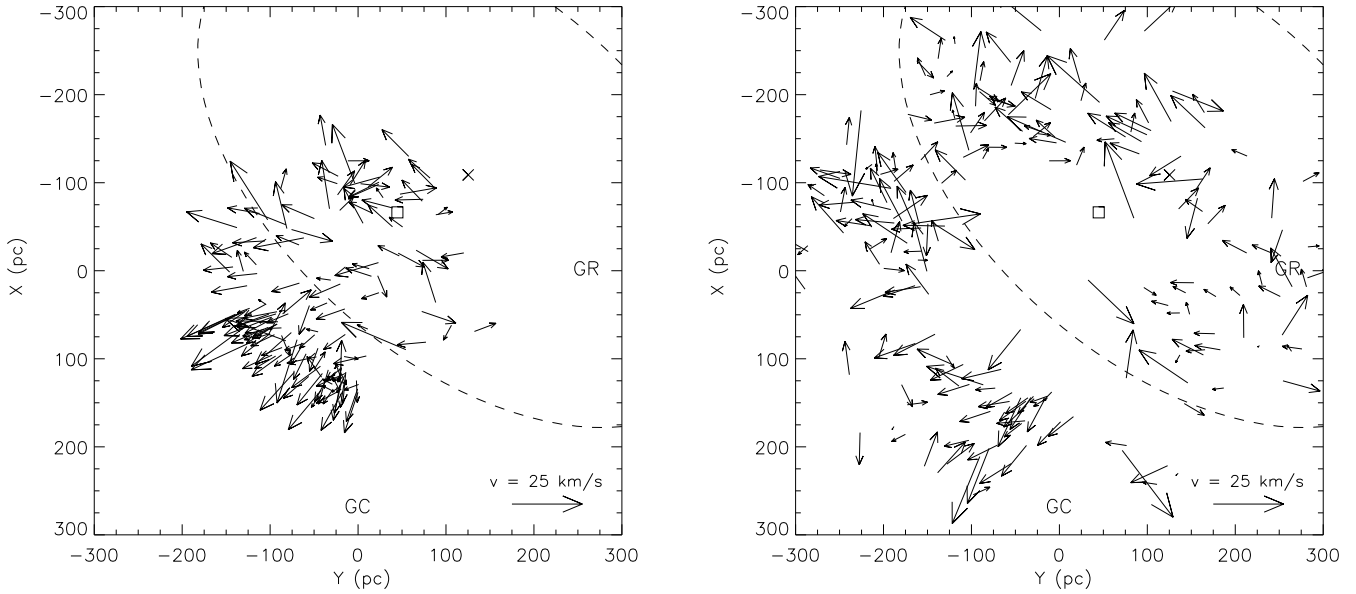


Fig. 15. Residual heliocentric space velocity vectors projected on the galactic plane for O and B stars with an age $\tau \leq 60$ Myr and $0 < R \leq 150$ pc (left) and $150 < R \leq 300$ pc (right). It is also drawn the Olano's (1982) Lindblad Ring (with a cross in its center) and the center of the Gould Belt (square) obtained by Comerón & Torra (1991). GC and GR indicate the galactic center and the galactic rotation directions respectively.

Two well-defined peaks in parallax seem to reinforce the nature of open cluster for these two entities, although the most distant is difficult to distinguish from the field stars because both the parallax and proper motion of its stars are close to those of field stars. On the other hand, Tr 10 was identified as an intermediate age OB association by de Zeeuw et al. (1999), who found 23 members spread over $\sim 8^\circ$ in the sky. Robichon et al. (1999) found 9 Hipparcos members of the cluster. The distance derived in both papers is the same (365 pc). The U velocity component found for the association is the same as for the cluster ($U = -27.3$ km s $^{-1}$), but there is a difference of 4 km s $^{-1}$ in the V component ($V_{\text{assoc}} = -17.8$ km s $^{-1}$, $V_{\text{clu}} = -21.9$ km s $^{-1}$).

We found that only 7 stars in this region ($225 < l \leq 285^\circ$, $100 < R \leq 300$ pc and $30 < \tau \leq 60$ Myr) have been identified by the above mentioned authors as members of open clusters or associations (including the list of de Zeeuw et al. 1999), so a large number of the remaining stars share the motion of these clusters and associations and are spread over a large region, as observed in Fig. 15. Finally, although IC 2391 and HR 3661 (= HIP 45189) seem to be isolated in Fig. 16, stars sharing the motion of these clusters were detected in our sample when the age interval was changed to $60 \leq \tau \leq 90$ Myr. This is in agreement with the estimated age for HR 3661 – 100 Myr (Platais et al. 1998) – but not with the age of IC 2391 – 30 Myr (Stauffer et al. 1997).

Further work will be necessary to confirm the existence of these streams and to deal with their origin in the context of the various models proposed for the Gould Belt. As

Table 7. Galactic coordinates and heliocentric velocity components of the clusters shown in Fig. 16. Units: l , b in degrees; R in pc; U , V and W in km s $^{-1}$.

Cluster	l	b	R	U	V	W
1. IC 2602 ²	289.6	-4.9	152	-8	-20	-0
2. a Car ¹	277.7	-7.6	132	-11	-24	-4
3. NGC 2232 ²	214.3	-7.7	325	-16	-12	-11
4. NGC 2516 ²	273.9	-15.9	346	-17	-24	-4
5. HR 3661 ¹	266.9	3.4	174	-22	-15	-6
6. IC 2391 ²	270.4	-6.9	146	-23	-14	-7
7. Tr 10 ²	262.8	0.6	365	-27	-22	-10
8. NGC 2451 ²	252.4	-6.8	189	-29	-20	-14

¹ Platais et al. (1998)

² Robichon et al. (1999)

an example, the fact that the (U, V) motion of the stream around IC 2451 A is very similar to the motion of an older (100-400 Myr) moving group independently detected by Figueras et al. (1997), Asiain et al. (1999a), Chereul et al. (1999) and Sabas (1997) raises interesting questions. As a starting point, the vertical motions of these structures should enable us to confirm or reject any relationship. In this way, Comerón (1999) has recently reported a systematic gradient in the vertical component of the velocity of those stars belonging to the Gould Belt along the galactic plane, which while being subtle is detectable in the Hipparcos astrometric data.

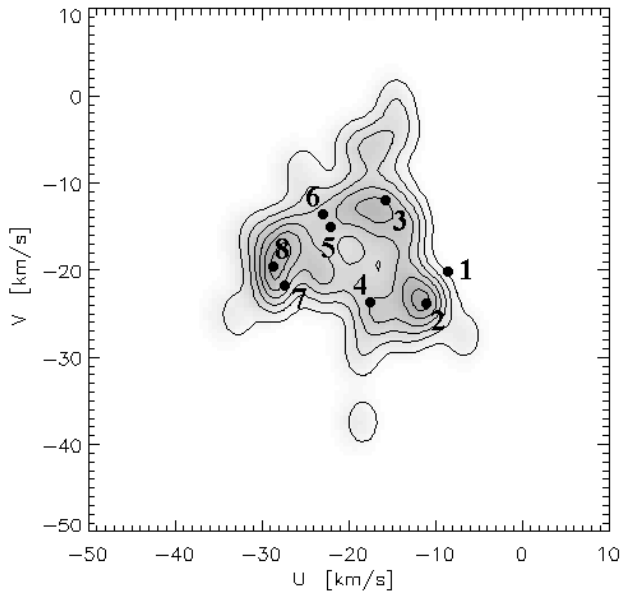


Fig. 16. Distribution of stars in the U - V plane – where a kernel estimator was used to indicate the lines of isocontours – for stars with $225 < l \leq 285^\circ$, $100 < R \leq 300$ pc and $30 < \tau \leq 60$ Myr. The filled circles correspond to the position of the clusters in Table 7.

5. Conclusions

A sample of O- and B-type stars with Hipparcos astrometric data, radial velocities and Strömgren photometry – from which photometric distances and ages were computed – has been used to study the spatial distribution and the kinematics of the young star system in the solar neighbourhood. Several numerical simulations have allowed us to assess the robustness of our methods and to evaluate the biases induced by the observational constraints.

The spatial distribution of the youngest and nearest group of stars is dominated by the presence of the Gould Belt. We found that this system extended up to 600 pc from the Sun and has an orientation with respect to the galactic plane of $i_G = 16$ - 22° and $\Omega_G = 275$ - 295° , depending on the distance and age intervals considered. For $R \leq 600$ pc, roughly 60% of stars younger than 60 Myr belong to the Gould Belt.

In the region with $R > 600$ pc, the stellar kinematics is dominated by the differential galactic rotation, since the Oort constants were found to be $A = 13.0 \pm 0.7$ km s $^{-1}$ kpc $^{-1}$, $B = -12.1 \pm 0.7$ km s $^{-1}$ kpc $^{-1}$, $C = 0.5 \pm 0.8$ km s $^{-1}$ kpc $^{-1}$ and $K = -2.9 \pm 0.6$ km s $^{-1}$ kpc $^{-1}$. In contrast, in the region with $R \leq 600$ pc, the Gould Belt dominates the kinematics of the youngest stars ($\tau \leq 60$ Myr), producing a decrease in the A and B Oort constants ($A \approx 6$ - 8 km s $^{-1}$ kpc $^{-1}$, $B \approx -(21$ - $14)$ km s $^{-1}$ kpc $^{-1}$) and an increase in C and K ($C \approx 5$ - 9 km s $^{-1}$ kpc $^{-1}$, $K \approx 4$ - 7 km s $^{-1}$ kpc $^{-1}$). This peculiar kinematics was also found

when those stars belonging to the Sco-Cen and Ori OB1 complexes were eliminated. Therefore, these associations are not the only responsible for these peculiarities, a finding which seems to reinforce the suggestion by Guillout et al. (1998b) that the Gould Belt is a disk-like rather than a ring-like structure.

A perfect agreement has been obtained when estimating the age of the Gould Belt system from the spatial distribution of the stars and from the study of the variations in the Oort constants with age. Taking into account the biases in the computation of individual photometric ages – stellar rotation and important uncertainties – we estimated an age of the Gould Belt inside the interval 30-60 Myr.

The study of the residual velocity field allowed us to estimate the cosmic dispersion for stars younger than ≈ 150 Myr. On the other hand, this residual velocity field for the youngest stars cannot be explained as an expansion from a point or a line. Moreover, the expansion motion classically attributed to the Gould Belt seems to be due to the nearest stars ($R \lesssim 300$ pc). In the region $300 < R \leq 600$ pc, we found that only Per OB2 has a clear residual motion away from the Sun. In the region with $100 \lesssim R \lesssim 300$ pc and $225 \lesssim l \lesssim 285^\circ$, two streams of stars with an age between 30 and 60 Myr have been found. One of these streams shares the motion of a Car (= HIP 45080) and IC 2602, whereas the other follows the motion of NGC 2451 A and Tr 10.

Acknowledgements. We thanked the anonymous referee for his comments and suggestions that have improved the quality of this paper. This study has been supported by the CICYT under contract ESP 97-1803 and by the PICS programme (CIRIT). DF acknowledges the FRD grant of the Universitat de Barcelona (Spain).

References

- Arenou, F., Luri, X. 1999, ASP Conference Series 167, ed. Daniel Egret and André Heck
- Asiain, R., Torra, J., Figueras, F. 1997, A&A 322, 147
- Asiain, R., Figueras, F., Torra, J., Chen, B. 1999a, A&A 341, 427
- Asiain, R., Figueras, F., Torra, J. 1999b, A&A 350, 434
- Balona, L.A., Shobbrook, R.R. 1984, MNRAS 211, 973
- Barbier-Brossat, M. 1997, private communication
- Binney, J., Merrifield, M. 1998 Galactic Astronomy, Princeton Series in Astrophysics, Princeton
- Bressan, A., Fagotto, F., Bertelli, G., Chiosi, C. 1993, A&AS 100, 647
- Brown, A.G.A., de Geus, E.J., de Zeeuw, P.T. 1994, A&A 289, 101
- Brown, A.G.A., Arenou, F., van Leeuwen, F., Lindegren, L., Luri, X. 1997, in: Proceedings of the Hipparcos-Venice'97 Symposium, ed. B. Battistich, ESA SP-402, 63
- Byl, J., Ovensen, M.W. 1981, MNRAS 196, 659
- Cabrera-Caño, J., Elias, F., Alfaro, E.J. 1999, in: Proceedings of the Conference Astrophysical Dynamics, Ap&SS, in press

If their spatial distribution shows an inclined structure, as obtained for young and distant stars, could our method, which does not take into account incompleteness effects, be capable to detect it?

- Related to the first point, for which scale height of the belts our method loses its statistical capability?
- Are the available number of stars enough to undertake this study? Can simulations provide a realistic estimate of the errors in the derived structure parameters?

To answer these questions simulated samples were built by considering the following steps:

- From each real star we generated a pseudo-star with the same age, visual magnitude and projected distance ($R \cos b$). Its galactic longitude was randomly assigned and the distance to the galactic plane (z) simulated following an exponential distribution with scale height Z_0 .
- Inside each age interval, the position of a fraction $q = 0.50$ of the generated pseudo-stars were rotated an angle $i_G = 20^\circ$ around the Y axis (galactic rotation direction), that is adopting $\Omega_G = 270^\circ$ for the ascending node of the Gould Belt.
- The process was repeated to generate samples with Z_0 values ranging from 40 to 80 pc (Mihalas and Binney 1981 quoted $Z_0 = 60$ pc for B-type stars).

An example of the spatial distribution of the generated pseudo-stars is presented in Fig. A1, which can be compared with the distribution of the real stars in Fig. 10. As seeked for, the same incompleteness effects are present in our simulated samples. The results after applying our resolution proces to the pseudo-stars with $V \leq 7$ and $R \leq 600$ pc are presented in Table A1, where in brackets we give the standard deviation for the 100 simulated samples.

First, we confirm that the angular halfwidths (ξ_G and ξ_g) correctly reflect the growth of the scale height (Z_0) of the simulated belts, the standard deviation of the differents samples ranging from 2° to 5° . The q parameter is also well recovered ($q = 0.50$), though with a standard deviation as large as 0.13-0.17. On the other hand, although the values obtained for the angles defining the Gould Belt's orientation (i_G , Ω_G) could indicate the presence of a small systematic trend when increasing Z_0 , probably due to the resolution process applied (Comerón 1992), it is always smaller than the standard deviation quoted. Looking at the interval $90 < \tau \leq 120$ Myr, where the observational incompleteness is more accentuated, we realize that when the presence of the inclined structure (the Gould Belt) is present in the simulated sample, only below the 2σ level we could obtain an i_G value as small as obtained from the real sample ($i_G = 3.4^\circ$). That is, there is a probability less than 5% to obtain inclinations about 4° in the worst case ($Z_0 = 80$ pc).

Table A1. Simulations on the Gould Belt's structural parameters. Results obtained after averaging 100 simulated samples with input values: $i_G = 20^\circ$, $\Omega_G = 270^\circ$, $q = 0.50$, with scale height: 40, 60 and 80 pc. Only pseudo-stars with $R \leq 600$ pc were considered.

Z_0	$i_G (^\circ)$	$\Omega_G (^\circ)$	q	$\xi_G (^\circ)$	$\xi_g (^\circ)$
$\tau \leq 30$ Myr					
40	21.4 _(3.0)	268.0 _(8.7)	0.50 _(0.15)	14.5 _(5.7)	15.7 _(5.7)
60	22.7 _(4.3)	268.5 _(13.2)	0.52 _(0.17)	19.3 _(5.7)	18.7 _(5.7)
80	21.6 _(5.2)	268.5 _(20.3)	0.51 _(0.13)	24.2 _(3.4)	24.2 _(3.4)
$30 < \tau \leq 60$ Myr					
40	21.1 _(2.8)	269.7 _(9.4)	0.50 _(0.13)	13.9 _(4.6)	13.9 _(4.0)
60	21.5 _(4.2)	270.1 _(15.9)	0.50 _(0.14)	18.7 _(4.6)	19.3 _(4.6)
80	22.3 _(5.7)	268.1 _(31.6)	0.49 _(0.15)	22.3 _(3.4)	23.0 _(2.9)
$60 < \tau \leq 90$ Myr					
40	21.1 _(3.9)	269.0 _(13.6)	0.50 _(0.16)	15.1 _(5.7)	15.7 _(5.2)
60	22.8 _(6.0)	269.3 _(22.5)	0.49 _(0.18)	19.3 _(5.7)	20.5 _(5.2)
80	22.8 _(7.6)	262.7 _(50.7)	0.50 _(0.15)	24.8 _(2.3)	24.8 _(2.9)
$90 < \tau \leq 120$ Myr					
40	20.9 _(4.4)	271.3 _(15.6)	0.49 _(0.17)	15.1 _(5.2)	16.3 _(5.2)
60	21.7 _(6.8)	269.1 _(36.3)	0.48 _(0.17)	20.5 _(5.2)	21.1 _(5.2)
80	24.7 _(8.4)	253.2 _(53.4)	0.50 _(0.16)	25.5 _(2.3)	25.5 _(2.9)

Appendix B: Simulations to check the kinematic analysis

Numerical simulations allow us to quantitatively evaluate the biases in the kinematic model parameters (Oort constants and solar motion components) induced by both, our observational constraints – irregular spatial distribution of the stars, incompleteness effects, availability of radial velocities, ... – and the presence of observational errors in the right hand side of Eqs. (3), (4) and (5), not considered in our least square fit. Here we present the procedure followed to generate the simulated samples, the results derived when using them to solve Eqs. (3), (4) and (5), and finally, the quantification of the biases present in our real sample resolution.

B.1. Process to generate the simulated samples

To take into account the irregular spatial distribution of our stars and their actual observational errors, parameters describing the position of the each simulated pseudo-star were generated as follow:

- From each real star we generated a pseudo-star that has the same nominal position (R_0, l, b) – not affected by errors – than the real one.
- We assumed that the angular coordinates (l, b) have negligible observational errors.
- If the star had a distance determination from the Hipparcos parallax, the parallax error of the pseudo-star has a distribution law:

$$\varepsilon(\pi) = e^{-\frac{1}{2} \left(\frac{\pi - \pi_0}{\sigma_\pi} \right)^2} \quad (\text{B1})$$

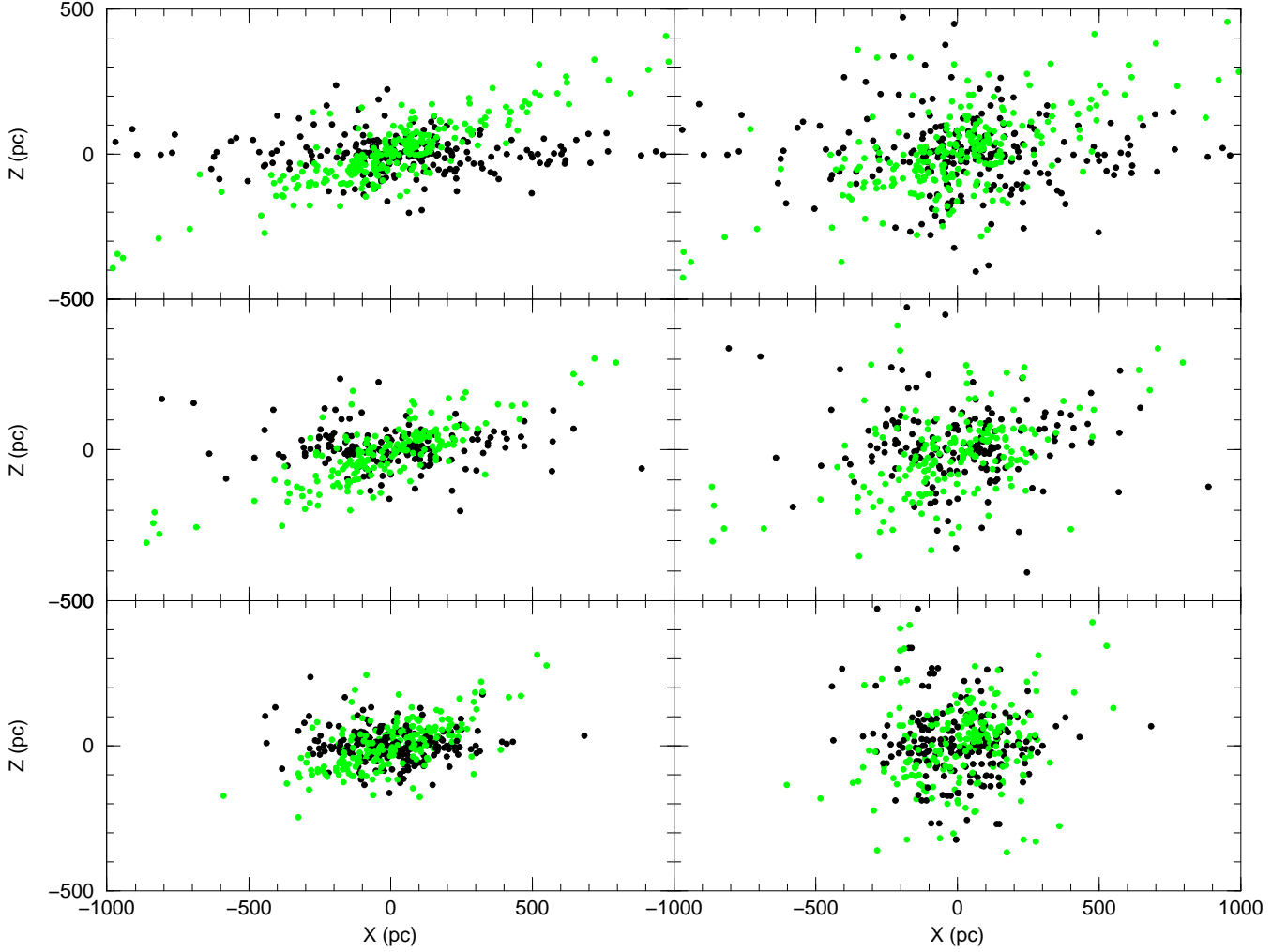


Fig. A1. Example of the distribution of the simulated samples on the X - Z galactic plane. At the top, the pseudo-stars with an age less than 30 Myr; in the middle, those with an age between 30 Myr and 60 Myr; and at the bottom, those with an age larger than 60 Myr. Left: Gould and Galactic plane generated with $Z_0 = 40$ pc; right: both generated with $Z_0 = 80$ pc.

where σ_π is the individual error in the parallax π_0 ($1/R_0$) of the real star. From the value of π affected by the error, the simulated distance affected by error ($R = 1/\pi$) was derived. On the other hand, if the star had a photometric distance determination, the error follows:

$$\varepsilon(R) = e^{-\frac{1}{2}\left(\frac{R-R_0}{\sigma_R}\right)^2} \quad (\text{B2})$$

where σ_R is the individual error in the photometric distance of the star.

To generate kinematic parameters we randomly assigned to each pseudo-star a velocity (U, V, W) by assuming a cosmic dispersion $(\sigma_U, \sigma_V, \sigma_W)$ and a Schwarzschild distribution:

$$\varphi'_v(U, V, W) = e^{-\frac{1}{2}\left(\frac{U-U_0}{\sigma_U}\right)^2 - \frac{1}{2}\left(\frac{V-V_0}{\sigma_V}\right)^2 - \frac{1}{2}\left(\frac{W-W_0}{\sigma_W}\right)^2} \quad (\text{B3})$$

where (U_0, V_0, W_0) are the reflex of solar motion. These components were transformed into radial velocities and proper motions in galactic coordinates using the nominal position of the pseudo-star (R_0, l, b) . The systematic motion due to galactic rotation was added following Eqs. (3), (4) and (5), obtaining the components (v_r, μ_l, μ_b) for each star. Finally, individual observational errors were introduced by using the error function:

$$\varepsilon(v_r, \mu_l, \mu_b) = e^{-\frac{1}{2}\left(\frac{v_r-v_{r0}}{\sigma_{v_r}}\right)^2 - \frac{1}{2}\left(\frac{\mu_l-\mu_{l0}}{\sigma_{\mu_l}}\right)^2 - \frac{1}{2}\left(\frac{\mu_b-\mu_{b0}}{\sigma_{\mu_b}}\right)^2} \quad (\text{B4})$$

where σ_{v_r} , σ_{μ_l} and σ_{μ_b} are the observational errors of the real star.

At the end of this process we had the following data for each pseudo-star: galactic coordinates (R, l, b) , velocity parameters (v_r, μ_l, μ_b) , errors in the velocity parameters $(\sigma_{v_r}, \sigma_{\mu_l}, \sigma_{\mu_b})$ and error in the trigonometric parallax (σ_π)

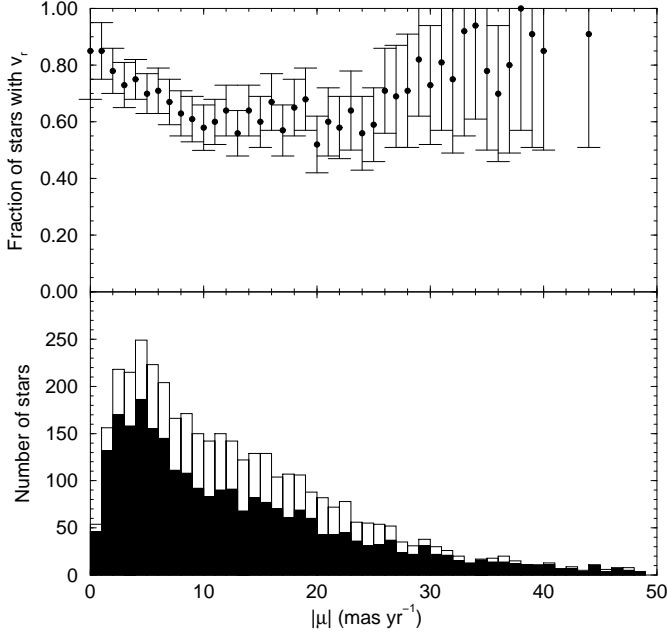


Fig. B1. Fraction of pseudo-stars with radial velocity (top) and distribution of the stars with proper motion (blank histogram) and radial velocity (filled histogram) (bottom) as a function of proper motion for one of the simulated samples (3915 stars). Error bars were estimated from a Poissonian error distribution.

or in the photometric distance (σ_R). The simulated radial component of those pseudo-stars generated from a real star without radial velocity was not used, thus we imposed in the simulated sample the same deficiency in radial velocity data that is present in our real sample (Sect. 2.2). The fraction of pseudo-stars with radial velocity against proper motion is shown in Fig. B1. This can be compared with Fig. 3 in Sect. 2.2 (the latter was made using the whole catalogue (6922 stars) whereas the former only contains the 3915 stars used in the fit of the Eqs. (3), (4) and (5)). The systematic trend present in the real sample is well reproduced in the simulations.

B.2. Results and discussion

Following this scheme, two sets of 100 simulated samples were built, each one having the same number of stars than the real sample. The first set was built adopting $K = 0 \text{ km s}^{-1} \text{ kpc}^{-1}$ and used to derive the kinematic parameters in the distance interval $600 < R \leq 2000 \text{ pc}$. For the interval $100 < R \leq 600 \text{ pc}$ we simulated the expansion by imposing $K = 5 \text{ km s}^{-1} \text{ kpc}^{-1}$. In Table B1 we show the adopted kinematic parameters. For the cosmic dispersion we considered $(\sigma_U, \sigma_V, \sigma_W) = (8, 8, 5) \text{ km s}^{-1}$ (see Sect. 4).

As can be seen in Table B1, three different resolution processes were undertaken:

- **Case 1:** A null error in distance was adopted. Therefore, the nominal distance of the pseudo-star is used ($R = R_0$) and only the effects of the errors on the radial velocity and proper motions are considered. No stars are rejected.
- **Case 2:** Errors in the radial velocity, proper motions and distance are considered. No stars are rejected.
- **Case 3:** As Case 2 but, to reproduce the real case, we rejected those stars with a residual velocity 3 times larger than the root mean square residual of the fit.

Case 1 allows to study the effect of the errors in radial velocity and proper motions, the incompleteness of our sample, the lack of radial velocity data (see Sect. 2.2) and the correlations between the different kinematic parameters to be determined. As we can see in Table B1, no systematic bias is present, the difference between the adopted values and the obtained ones never exceeding 0.2 km s^{-1} for the solar motion components and $0.2 \text{ km s}^{-1} \text{ kpc}^{-1}$ for the Oort constants.

When the error in the distance is considered (Case 2) the most noticeable effect is a clear bias in the A and B Oort constants. For A and the radial velocity resolution, a bias of $+(0.6-0.7) \text{ km s}^{-1} \text{ kpc}^{-1}$ was obtained. On the contrary, from the proper motion equations this bias was $-(0.7-0.8) \text{ km s}^{-1} \text{ kpc}^{-1}$. For the combined resolution, and due to the larger number of proper motion equations ($2N$ against N), the bias was $-(0.1-0.5) \text{ km s}^{-1} \text{ kpc}^{-1}$, depending on the distance interval considered. For B constant, a bias of $+(0.7-0.9) \text{ km s}^{-1} \text{ kpc}^{-1}$ was found from proper motion data. Apart from the distance errors, other effects contribute to the biases detected: the specific decreasing distribution on distance of our real sample (well reproduced in the simulations) and the distance cut applied in the resolution process (100, 600, 2000 pc).

In Case 3, to mimic the real case, those stars with a residual velocity larger than 3 times the root mean square residual were rejected. In the simulated samples there are not high velocity stars, but in the reality it will be a few percentage of kinematically peculiar stars, or stars with non-well determined errors in the distance or in the velocity components. We confirm that our rejection criterion do not induced any additional bias, showing only an expected decrease in the χ^2 statistic.

Concluding, these simulations allow us to estimate which biases are expected in the kinematic parameters obtained from our real sample. As we can see, for $100 < R \leq 600 \text{ pc}$ our results for the combined solution can be biased on $\approx -0.5 \text{ km s}^{-1} \text{ kpc}^{-1}$ in A Oort constant and $\approx -0.8 \text{ km s}^{-1} \text{ kpc}^{-1}$ in B , whereas for C and K is negligible. For the solar motion components a bias about $0.3-0.4 \text{ km s}^{-1}$ can be present. For $600 < R \leq 2000 \text{ pc}$ the bias for A , C and K is negligible while a positive bias of $\sim 0.9 \text{ km s}^{-1} \text{ kpc}^{-1}$ is found for B . Again, for solar motion a bias of $0.3-0.4 \text{ km s}^{-1}$ is expected in each component.

Table B1. Mean Oort constants and residual solar motion for 100 simulated samples obtained solving Eq. (3) for radial velocities, Eqs. (4) + (5) for proper motions and Eqs. (3) + (4) + (5) for the combined solution. The standard deviation for the 100 samples is shown in brackets. Units: A , B , C , K in $\text{km s}^{-1} \text{ kpc}^{-1}$; U_\odot , V_\odot , W_\odot , σ in km s^{-1} . χ^2/N_{eq} is the value of χ^2 divided by the number of equations.

Radial velocities								
100 < $R \leq 600$ pc					600 < $R \leq 2000$ pc			
Adopted	Case 1	Case 2	Case 3	Adopted	Case 1	Case 2	Case 3	
A	14.0	13.9 _(1.8)	14.7 _(1.6)	14.7 _(1.7)	14.0	13.9 _(0.7)	14.6 _(0.8)	14.5 _(0.8)
C	0.0	0.2 _(1.6)	-0.1 _(1.7)	-0.1 _(1.7)	0.0	-0.1 _(0.6)	0.1 _(0.7)	0.1 _(0.7)
K	5.0	4.8 _(1.1)	4.9 _(1.2)	4.9 _(1.2)	0.0	-0.1 _(0.4)	-0.3 _(0.9)	-0.3 _(0.5)
U_\odot	9.0	9.0 _(0.5)	9.1 _(0.4)	9.1 _(0.5)	9.0	8.9 _(0.8)	8.8 _(0.9)	8.8 _(0.9)
V_\odot	12.0	12.1 _(0.6)	12.2 _(0.5)	12.2 _(0.6)	12.0	12.1 _(0.7)	11.6 _(0.7)	11.6 _(0.7)
W_\odot	7.0	7.2 _(1.0)	7.2 _(1.0)	7.3 _(1.0)	7.0	7.0 _(1.8)	6.7 _(1.8)	6.7 _(1.7)
σ		8.4 _(0.2)	8.5 _(0.2)	8.4 _(0.3)		8.3 _(0.3)	9.2 _(0.4)	9.0 _(0.4)
χ^2/N_{eq}		1.00	1.00	0.97		1.00	1.11	1.06
Proper motions								
100 < $R \leq 600$ pc					600 < $R \leq 2000$ pc			
Adopted	Case 1	Case 2	Case 3	Adopted	Case 1	Case 2	Case 3	
A	14.0	14.2 _(0.8)	13.2 _(0.8)	13.2 _(0.8)	14.0	14.0 _(0.5)	13.3 _(0.5)	13.3 _(0.5)
B	-12.0	-12.0 _(0.7)	-11.3 _(0.7)	-11.3 _(0.7)	-12.0	-12.0 _(0.4)	-11.1 _(0.4)	-11.1 _(0.4)
C	0.0	0.1 _(0.8)	-0.1 _(0.8)	-0.1 _(0.8)	0.0	0.0 _(0.5)	-0.1 _(0.6)	-0.1 _(0.6)
K	5.0	5.2 _(1.8)	4.8 _(1.8)	4.8 _(1.9)	0.0	0.1 _(2.1)	-0.2 _(2.1)	-0.3 _(2.1)
U_\odot	9.0	9.0 _(0.2)	8.6 _(0.2)	8.6 _(0.2)	9.0	9.0 _(0.6)	8.7 _(0.7)	8.7 _(0.7)
V_\odot	12.0	12.0 _(0.2)	11.4 _(0.2)	11.4 _(0.2)	12.0	12.1 _(0.6)	11.4 _(0.7)	11.4 _(0.7)
W_\odot	7.0	7.0 _(0.1)	6.6 _(0.1)	6.6 _(0.1)	7.0	7.1 _(0.3)	6.7 _(0.3)	6.7 _(0.3)
σ		6.4 _(0.1)	6.6 _(0.1)	6.6 _(0.1)		7.6 _(0.2)	7.8 _(0.2)	7.6 _(0.2)
χ^2/N_{eq}		1.00	0.94	0.91		1.00	0.91	0.88
$(\chi^2/N_{\text{eq}})_l$		1.00	0.93	0.90		1.00	0.87	0.83
$(\chi^2/N_{\text{eq}})_b$		1.00	0.94	0.91		1.00	0.96	0.93
Combined solution								
100 < $R \leq 600$ pc					600 < $R \leq 2000$ pc			
Adopted	Case 1	Case 2	Case 3	Adopted	Case 1	Case 2	Case 3	
A	14.0	14.1 _(0.7)	13.5 _(0.7)	13.5 _(0.7)	14.0	14.0 _(0.6)	13.9 _(0.5)	13.9 _(0.5)
B	-12.0	-12.0 _(0.7)	-11.2 _(0.7)	-11.2 _(0.7)	-12.0	-12.0 _(0.6)	-11.1 _(0.4)	-11.2 _(0.4)
C	0.0	0.1 _(0.7)	0.2 _(0.7)	0.2 _(0.7)	0.0	-0.0 _(0.5)	0.1 _(0.4)	0.1 _(0.4)
K	5.0	5.0 _(0.8)	5.1 _(0.8)	5.1 _(0.9)	0.0	-0.1 _(0.5)	-0.2 _(0.4)	-0.2 _(0.4)
U_\odot	9.0	9.0 _(0.2)	8.7 _(0.2)	8.7 _(0.2)	9.0	9.0 _(0.7)	8.8 _(0.5)	8.7 _(0.5)
V_\odot	12.0	12.0 _(0.2)	11.6 _(0.2)	11.6 _(0.2)	12.0	12.1 _(0.6)	11.6 _(0.5)	11.6 _(0.5)
W_\odot	7.0	7.0 _(0.1)	6.7 _(0.1)	6.7 _(0.1)	7.0	7.1 _(0.4)	6.7 _(0.3)	6.7 _(0.3)
σ		6.7 _(0.1)	6.7 _(0.1)	6.6 _(0.1)		10.2 _(0.2)	8.1 _(0.2)	8.0 _(0.2)
χ^2/N_{eq}		1.00	0.95	0.92		1.00	0.97	0.93
$(\chi^2/N_{\text{eq}})_r$		1.00	1.00	0.97		1.00	1.12	1.08
$(\chi^2/N_{\text{eq}})_l$		1.00	0.93	0.90		1.00	0.98	0.84
$(\chi^2/N_{\text{eq}})_b$		1.00	0.94	0.91		1.00	0.96	0.93